Rab11B is required for binding and entry of recent H3N2, but not H1N1, influenza A isolates

Allyson H. Turner[1,#], Sara A. Jaffrani[1,#], Hannah C. Kubinski[1,a], Deborah P. Ajayi[1,2], Matthew B. Owens[1,2], Conor D. Fanuele[1], Madeline P. McTigue[1,2], Cailey L. Appenzeller[1], Addington Bowling[1], Hannah W. Despres[1,2,b], Madaline M. Schmidt[1,c], Dave J. Shirley[3], Jessica W. Crothers[4], Ramiro Barrantes-Reynolds[1], Emily A. Bruce[1,*]

[1]Department of Microbiology and Molecular Genetics, University of Vermont, Burlington, Vermont, USA

[2]Cellular, Molecular, and Biomedical Sciences Graduate Program, University of Vermont Larner College of Medicine, Burlington, VT, USA

[3]Faraday, Inc. Data Science Department, Burlington, Vermont, United States of America

[4]Department of Pathology and Laboratory Medicine, University of Vermont, Burlington, VT, USA

[a]Molecular Genetics and Microbiology Graduate Program, Duke University, Durham, North Carolina, USA

[b]Department of Microbiology and Immunology, University of Maryland School of Medicine, Baltimore, Maryland, USA

[c]Microbiology and Molecular Genetics Graduate Program, Emory University, Atlanta, Georgia, USA

[#]These authors contributed equally to this work.

*Correspondence to Dr. Emily Bruce, Emily.bruce@med.uvm.edu

ABSTRACT

As an obligate intracellular parasite, influenza A virus (IAV) depends on host proteins to complete several important functions, including trafficking viral proteins throughout the cell. Previous work has established a critical role for the cellular vesicular trafficking protein, Rab11A, in transporting the viral genome segments to the site of budding at the plasma membrane. While the role of Rab11A in IAV assembly is relatively well understood, very little is known about the function of a closely related isoform (Rab11B) during influenza virus infection. We have shown that both Rab11A and Rab11B are required for successful IAV infection by current H1N1 or H3N2 isolates. Cells in which either Rab11A or Rab11B were depleted failed to efficiently produce virus, with significant reductions in infectious titer. Surprisingly, our data revealed that recent (2022) H3N2, but not H1N1, isolates failed to efficiently produce viral proteins in single-cycle infections when Rab11B (but not Rab11A) was depleted. Flow cytometry analysis suggests that the defect in protein production is driven by a reduction in the total number of infected cells, rather than a decrease in viral protein production at the single cell level. Using reverse genetics and '7+1' reassortant viruses we mapped this Rab11B-dependent early defect in recent H3N2 isolates to the HA gene. RT-qPCR analysis of H3N2 virions bound to the cell surface showed a ~50% decrease in virus binding the surface of cells depleted of Rab11B, but not Rab11A. This data suggests a novel role for Rab11B during viral entry, likely at the stage of viral binding, that is specific to H3N2 isolates.

INTRODUCTION

Influenza A virus (IAV) is a highly infectious pathogen, causing seasonal epidemics that result in around three to five million severe cases each year, in addition to causing periodic pandemics that emerge from novel IAV strains[1,2]. While there are many different subtypes of IAV, currently there are only two which are circulating within the human population, H1N1 and H3N2[3]. Influenza owes much of its pandemic potential to the fact that its genome is composed of eight distinct segments which can mix to form novel

genetic combinations in a cell infected with two influenza viruses simultaneously, a process known as reassortment[4].

As a segmented negative strand RNA virus, influenza encodes at least 14 proteins on its eight segments[3]. After transcription and translation, these proteins collectively carry out the functions required to complete the viral life cycle within a host cell. Cellular entry of the influenza virion is mediated by the viral glycoprotein hemagglutinin (HA) binding to sialic acid moieties on the cell surface, which is thought to trigger receptor mediated endocytosis[5,6]. Broadly speaking, influenza viruses that infect human cells are thought to bind to α2,6 sialic acid modifications on cell surface proteins, differentiating them from avian viruses which are thought to prefer α2,3 sialic acids [reviewed in[3,4,7]]. The classical model of influenza binding continues to be refined and expanded however, through new work that suggests there may be subtype-specific effects and both the identity of the sialylated protein and its cell surface density may play important roles[8–15]. Specific characteristics of the sialic acid modifications itself can also affect binding, with more recent H3N2 isolates preferring a highly branched structure[16]. Intriguingly H3N2s have shown decreased avidity for α2,6 sialic acid from 1968-2010 which correlates with a decrease in infection severity and evidence that NA contributed to mediating receptor binding[17]. After viral binding, internalization occurs through an incompletely understood process that is likely to involve signaling from one or more cell surface proteins and may require specific 'internalization receptors' [reviewed in[18,19]].

After endocytosis, the lowered pH of the endosome triggers a conformational change in HA which mediates fusion between viral and cellular membranes[20–23]. The acidic environment of the endosome also triggers activation of the matrix 2 protein (M2) ion channel, which transports protons to the interior of the virion, resulting in disassociation of M1 from the ribonucleoprotein complexes (RNPs) that is required for their subsequent nuclear import[24]. Once released into the cytoplasm, the RNP complexes that comprise the genome segments are transported to the nucleus where influenza genome replication occurs. During late stages of viral infection newly produced genome segments (vRNPS) comprising full length negative sense RNA molecules are coated with nucleoprotein (NP)

85 and bound to the polymerase complex composed of the polymerase basic protein 1 (PB1),
86 polymerase basic protein 2 (PB2) and the polymerase acidic protein (PA) and then exported
87 from the nucleus. Once in the cytoplasm, vRNPs must traffic to the site of budding at the
88 plasma membrane before being released in newly formed virions to start the cycle of
89 infection anew[25].

90 The process of transporting the vRNPs during this stage is highly dependent on the
91 cellular Rab11 pathway, which is co-opted during viral infection to coordinate the apical
92 transport of the influenza genome[26–28]. Rab11 is a member of the Rab GTPase family, and
93 plays a key role in vesicular transport within the recycling endosome pathway[29]. A direct
94 interaction between Rab11A and PB2 (a component of the influenza tripartite polymerase
95 complex) mediates binding between Rab11A and negative sense vRNPs, with no binding
96 observed to full length positive sense or viral mRNA species[26,30]. This interaction is
97 hypothesized to disrupt the binding of Rab11-Family Interacting Proteins (FIPs), possibly
98 through Rab11's regulatory Switch I region[30]. Influenza infection disrupts the normal
99 functioning of the endosomal trafficking pathway to favor transport of vRNPs to the plasma
100 membrane[31–33]. During transport, large clusters of multiple genome segments that
101 colocalize with Rab11 can be observed by fluorescent *in situ* hybridization[26]. This Rab11
102 dependent transport serves to concentrate and cluster the eight IAV segments in defined
103 subcellular sites, dependent on microtubules[34–39]. Finally, Rab11 is known to play a role in
104 the very late stages of the viral life cycle. Rab11 can traffic vRNPs between cells through
105 tunneling nanotubules, allowing for cell to cell spread without generation of complete
106 virions[40]. Cells lacking Rab11 fail to produce filamentous virions and exhibit signs of
107 budding defects, possibly due to a secondary failure to transport the viral genome to the
108 site of budding[41].

109 Notably, the majority of this research has been focused exclusively on the role of
110 Rab11A, while a small subset of studies looked at the combined effect of Rab11A and
111 Rab11B. Studies examining the role of the different Rab11 isotypes, in the context of
112 cancer, reveal the two isoforms can play distinct roles, leading us to wonder if there might
113 also be differences in how they interact with viral proteins during the IAV lifecycle[42]. While

114 the exact binding site between PB2 and Rab11A is unknown, the interaction between these
115 proteins is completely abolished by mutations to the C-terminal Class I switch region, an
116 area that is highly conserved between the different Rab11 family members[30]. This data,
117 along with a previously reported drop in titer from A549 cells depleted of Rab11B and
118 infected with PR8, suggested to us that Rab11B might play a similar role as Rab11A during
119 influenza infection, though this phenotype did not extend to HEK-293T cells[41]. As the
120 majority of studies examining the role of Rab11 in influenza infection have utilized older
121 (often lab-adapted) strains, we were also curious about whether the requirement for Rab11
122 extended to currently circulating strains of influenza A. Here we show that both Rab11A
123 and Rab11B are required for efficient production of infectious virions from seasonal H1N1
124 and H3N2 subtypes circulating in 2022. As expected, Rab11A played a role late in infection
125 (i.e., post protein production) for both subtypes. Surprisingly, we discovered that Rab11B is
126 required early in the life cycle of H3N2 infection, with cells lacking Rab11B failing to
127 efficiently produce viral proteins. We were able to map this defect specifically to the HA
128 gene and trace it to a defect early in viral entry, as H3N2 (but not H1N1) virions fail to bind
129 to the surface of cells lacking Rab11B. Our findings suggest a surprising new role for one of
130 the two highly conserved Rab11 isoforms in influenza infection and highlights a clear role
131 of differential requirements for viral binding and entry of recent H1N1 vs H3N2 subtypes.
132

133 **RESULTS**

134 To determine the effect Rab11A and Rab11B played on the replication of current
135 seasonal influenza viruses, we used siRNAs targeting each gene to transiently knockdown
136 expression in human adenocarcinoma alveolar basal epithelial (A549) cells, in the hopes of
137 minimizing off-target effects that can occur with stable knockdown/knockout. In addition
138 to Rab11A and Rab11B, we included a third Rab (Rab8A) that is also involved in recycling
139 endosome trafficking but is not known to impact influenza viral replication, as well as a
140 non-targeting control. To verify the efficiency of our knockdown, we initially used western
141 blot to measure Rab11 protein expression, relative to a house keeping gene (β-actin). We
142 observed global Rab11 protein depletion using a non-isoform specific antibody in cells

143 treated with siRNA targeting both Rab11A and Rab11B (Figure 1A). Using a Rab11A isoform
144 specific antibody, we could see depletion of Rab11A in cells treated with siRNA to Rab11A
145 (or Rab11A and B in combination) (Figure 1B). However, due to difficulties in antibody
146 sensitivity when detecting endogenous protein levels we used RT-qPCR to quantify gene
147 expression, relative to a house-keeping transcript (18S) and expression in a NT control at 48
148 hrs post transfection. Our RT-qPCR results (Figure 1C) verified Rab11A gene expression
149 was reduced to about 15% of endogenous levels, Rab11B to ~5% and Rab8 to ~20%. For
150 cells in which we simultaneously depleted Rab11A and Rab11B, we used the same total
151 amount of RNA (i.e., half the level/gene for a single knockdown) to avoid cell toxicity. In this
152 case, depletions were slightly less efficient, with Rab11A gene expression reduced to ~20%
153 and Rab11B to ~10% (Figure 1C).
154 Having confirmed the efficiency of our depletions, we then challenged each
155 depleted condition using two different, recent, low passage IAV isolates,
156 A/Burlington/UVM-0478/2022 (H1N1) (denoted in this study as UVM-0478) and
157 A/Burlington/UVM-1927/2022 (H3N2) (denoted here as UVM-1927) to perform single cycle
158 infections. As predicted, we found that cells in which either or both Rab11A/Rab11B were
159 depleted resulted in a significant reduction in plaque forming units (PFU) of virus produced
160 during infection. We saw a ~3-5 fold reduction in viral titer in cells lacking Rab11A or
161 Rab11B and a further drop in cells lacking Rab11A+B (7-10 fold), in cells infected with
162 either UVM-0478 (Figure 1D) or UVM-1927 (Figure 1E). In cells depleted of Rab8A and
163 infected with UVM-0478 we saw a small but consistent drop in titer (~2 fold) while UVM-
164 1927 replication was unaffected (raw viral titers in Figure S1).
165 To verify the drop in titer observed was due to the previously characterized role of
166 Rab11 in late stage RNP trafficking, we then examined the viral protein production of
167 infected cells in our knockdown conditions. We observed no significant effect on viral
168 protein expression in cells infected with UVM-0478 (Figure 2A) after densitometry
169 quantification was used to determine the levels of HA0, NP, or M2 (Figure 2B-D) normalized
170 to the cellular housekeeping gene, GAPDH (or alternatively, normalized to β-actin, Figure
171 S2). Unexpectedly, we observed a significant drop in viral protein production in cells

172 depleted of Rab11B that were infected with UVM-1927 (Figure 2E). Expression of HA0, NP,
173 and M2 (Figure 2F-H) was reduced to 25% of that seen in cells treated with the NT control.
174 Surprisingly, this defect in viral protein production was partially rescued in cells
175 simultaneously depleted of Rab11A and Rab11B. In order to determine if this rescue was
176 due to less efficient knockdown (as cells treated with siRNA to Rab11A and B
177 simultaneously received half the total siRNA that was used in individual knockdowns), we
178 treated cells with a half dose of Rab11A or Rab11B siRNA (along with a non-targeting
179 control) before infecting them with UVM-1927 as above. The failure to produce viral
180 proteins was not affected by lowering the siRNA dose, with cells lacking Rab11B once
181 again producing 80-90% less HA, NP and M2 (Figure S3). Given prior reports of reciprocal
182 functions in the Rab11A and Rab11B isoforms, this finding suggests that Rab11A and B
183 could also be playing opposing functions in the context of H3N2 entry[42,43].
184 To broaden our conclusions, we obtained a second 2022 H3N2 from a different
185 geographical region, A/Baltimore/JH-0586/2022 (H3N2) (referred to in this study as JH-
186 0586). JH-0586 is genetically distinct from UVM-1927, with more than 100 nucleotide level
187 differences across the eight segments of the two viruses. Like UVM-1927, JH-0586 also
188 depended on the Rab11 isoforms to produce infectious virus, with a particular dependence
189 on Rab11B, as observed above with UVM-1927 (Figure 3A). The loss of Rab11B resulted in a
190 five-fold drop in viral titer while the simultaneous depletion of Rab11A and Rab11B resulted
191 in a 20-fold decrease, while Rab8A depletion did not affect viral replication. In line with our
192 prior observations, viral protein production was also substantially decreased in cells
193 lacking Rab11B (Figure 3B). Quantification revealed this trend was most pronounced in
194 expression of NP (85% of NT) and M2 (~50%), while HA0 expression was decreased to a
195 lesser extent (~15%) (Figure 3C-E). Simultaneous depletion of Rab11A and Rab11B again
196 appeared to, at least partially, rescue the defect induced by the loss of Rab11B alone.
197 Finally, Rab8A depletion did not alter the expression of viral protein levels, compared to the
198 NT control.
199 To determine if this phenotype was restricted to A549 cells, we next expanded our
200 study to include NCI-H441 (H441) cells, an immortalized human 'club cell'-like line. To rule

201 out off-target effects of the siRNA constructs/depletion strategy we had used in A549 cells,
202 we used lentiviral transduction to create a stable cell line with a doxycycline-driven
203 inducible shRNA targeting Rab11B. We achieved high (~90%) levels of Rab11B depletion in
204 these cells three days after induction (Figure 4A), allowing us to examine viral protein
205 production of UVM-1927 after a single round of replication (Figure 4B). Expression of HA,
206 NP and M2 was once again significantly (<50%) decreased in cells induced with Rab11B
207 shRNA constructs (Figure 4C-E), suggesting the dependence of recent H3N2 isolates on
208 Rab11B was not an artifact of either cell type or our depletion strategy.
209 Next, we wanted to understand whether our phenotype was being driven by a global
210 drop in the number of cells being infected, or if the same number of cells were infected but
211 each produced fewer viral proteins. As western blots of total cell lysates are unsuited to
212 analyzing protein production at a single cell level, we used flow cytometry to measure HA
213 and M2 expression in individual cells that had been treated with siRNAs targeting Rab11A,
214 Rab11B or a NT control and infected with UVM-1927 as above. The infected control cells
215 were clearly visualized as a second peak (Figure 5, light gray) with greater levels of staining
216 than the mock infected cells (dark gray, single left-most peak) after staining with both anti-
217 H3N2 serum and an M2 antibody (Figure 5A, B). As expected for a multiplicity of infection
218 (MOI) of 1 (chosen due to relatively low titers of our low passage stocks), infected cells
219 were roughly a third of the cell population. Unsurprisingly, given our prior data, the loss of
220 Rab11A did not alter viral protein expression patterns (Figure 5A, B; compare maroon to
221 light gray line). In cells lacking Rab11B, the total number of cells expressing viral proteins
222 was reduced ~50%, while we observed similar intensity of viral protein expression in the
223 positive cell population (Figure 5A, B; compare how purple line is decreased along the *y*-
224 axis dimension [count] but not the *x*-axis [viral antigen intensity]). Quantification of multiple
225 biological replicates revealed a ~50% drop in the number of cells infected (i.e., producing
226 viral proteins) when Rab11B was knocked down, compared to both the NT control and the
227 Rab11A knockdown (Figure 5C). Further analysis of viral protein expression within the
228 infected cell population showed no decrease in HA or M2 expression (Figure 5D, E). This
229 assay revealed a significant defect in the number of Rab11B depleted cells able to produce

230 viral proteins, rather than a broad dampening of protein expression. This suggested that if a
231 cell was able to make viral proteins at all then it would produce the normal amount,
232 implying a defect upstream of translation.

233 As our data suggested that protein (and likely RNA) production was unaffected by
234 Rab11B depletion, we hypothesized that the infection defect in these cells was occurring
235 somewhere in the entry process. To look at the kinetics of entry we used a 'time of addition'
236 assay in which we added ammonium chloride at specific timepoints post infection to stop
237 endosomal acidification and thus viral fusion[44]. Infections were allowed to progress in the
238 presence of ammonium chloride, and the percentage of infected cells was measured by
239 flow cytometry sixteen hours later (Figure 6A). In cells treated with the NT control, we saw
240 no escape from the endosome when ammonium chloride was added concurrently with
241 viral inoculum (Figure 6B). The majority of viral fusion appeared to occur between 20 and 60
242 minutes, consistent with previously reported half-times for influenza viral entry[44]. Cells
243 lacking Rab11A showed no defect in entry kinetics, with an equal or greater number of cells
244 infected throughout the measured time course (Figure 6B, C). In Rab11B depleted cells, we
245 observed a significant drop in the number of infected cells at 45, 60 and 90 minutes
246 compared to the NT control (Figure 6B, C). To better visualize whether the Rab11B entry
247 kinetics were delayed compared to NT (which could imply utilization of an alternative
248 trafficking pathway) we normalized the percent of infected cells to those infected in the NT
249 control at each timepoint (Figure 6D). This revealed that cells lacking Rab11B had
250 significant defects in their ability to support normal viral entry, but the rate of entry itself
251 was not delayed compared to the NT control (Figure 6D), with a near constant drop in
252 number of infected cells at each of the later timepoints compared to NT (Figure 6E).

253 Given the profound defects we observed in overall entry, we next sought to
254 determine which viral gene (or genes) contributed to the singular dependence of our H3N2
255 viruses on Rab11B. Viral binding is governed primarily by HA (with a possible role for NA)
256 with fusion dependent on HA, uncoating relying on M2, and transport to the nucleus likely
257 mediated by multiple genes. After first verifying that A/Puerto Rico/8/1934 (H1N1, referred
258 to as PR8 in future) was not dependent on Rab11B for viral protein production (Fig 7A-D),

259 we created 7+1 reassortments of the UVM-1927 HA or NA gene segments in a PR8
260 background using an established reverse genetics system. The PR8 7+1 reassortant
261 containing the UVM-1927 HA gene (PR8: HA_UVM-1927) showed a significant (75-90%)
262 reduction in viral protein levels when HA, NP and M2 expression was quantified in cells
263 lacking Rab11B (Figure 7E-H). Conversely, no significant reduction in viral protein
264 expression was seen in 7+1 reassortant containing the UVM-1927 NA gene (Figure 7I-L).
265 This data shows that the dependence on Rab11B for viral protein production can be
266 mapped to the HA segment, and to the HA protein itself given that segment 4 is
267 monocistronic[45]. This result strongly suggested that Rab11B is required at one of the
268 earliest stages of entry, given that HA plays key roles in binding and fusion.
269 To explore our hypothesis that Rab11B was acting at the earliest stages of entry, we
270 used an RT-qPCR based assay to examine how the rate of binding was affected by
271 depletion of Rab11B. We adapted an assay that we have previously used to measure levels
272 of Hantavirus binding[46], in which we synchronized viral binding to the surface of cells by
273 binding at 4°C to prevent endocytosis. We then washed cells to remove unbound virions
274 and used RT-qPCR to measure the viral genome copies of UVM-1927 (H3N2) attached to
275 cells after one hour. To verify that we were measuring authentic bound virus (rather than
276 virus sticking non-specifically to cells or plastic), we used exogenous neuraminidase (NA)
277 to cleave bound virus, as NA plays a key role in cleaving sialic acids to release newly
278 produced virions that would otherwise remain attached to the producer cell[21]. Using this
279 control, we found a significant drop in viral binding, with ~97% of viral RNA removed upon
280 NA treatment (Figure 8A). Having confirmed we were detecting authentically bound virions,
281 we next conducted the binding experiment with UVM-1927 in cells lacking Rab11A or
282 Rab11B. Notably, in cells lacking Rab11B we observed a significant (~50%) decrease in
283 binding compared to cells treated with a NT control, while binding of virions in cells
284 depleted of Rab11A was unaffected (Figure 8B). Next, we repeated this experiment using
285 the UVM-0478 (H1N1) virus, to confirm that the binding defect was specific to the scenario
286 in which viral protein production failed to occur. In this scenario, cells lacking Rab11B had

287 no defect in viral binding (Figure 8C), suggesting that the ability of Rab11B to support viral
288 binding is specific to H3N2 viruses, and is dispensable for the binding of this H1N1 isolate.

289 **DISCUSSION**

290 The data presented here are consistent with a model in which recently circulating
291 H1N1 and H3N2 influenza subtypes bind to different cellular receptors or attachment
292 factors. In this framework, the H3N2 receptor(s) is trafficked by Rab11B, while the H1N1
293 receptor(s) is transported by a non-Rab11A/B dependent mechanism (Figure 9). While we
294 were initially surprised to observe such different roles for these two Rab11 isoforms in the
295 context of influenza infection, prior literature does support the isoforms playing distinct
296 and even opposing functions within the cell, despite their sequence similarity[42,43]. To some
297 degree, the distinct functions of Rab11A and Rab11B are a result of differential expression,
298 where Rab11A is ubiquitously expressed while Rab11B is enriched in the brain, testis and
299 heart (while having a lower but broad level of expression in other tissues)[43]. And in many
300 cases, Rab11A and Rab11B can transport the same cargo, functioning in a redundant
301 manner[47].

302 However, there are also examples of Rab11A and Rab11B playing distinct roles
303 within the same cellular background. Rab11B plays a role in trafficking fibroblast growth
304 factor receptor 4 (FGFR4) that is different and distinct from Rab11A's role in this pathway[48],
305 and Rab11B but not A have been implicated in transport of the cystic fibrosis
306 transmembrane conductance regulator (CFTR)[49]. Notably Rab11B (but not Rab11A) is
307 critical for recycling the Protease-activated receptor-1 (PAR1) while enhanced degradation
308 of PAR1 observed in cells lacking Rab11B is blocked by simultaneous depletion of
309 Rab11A[43]. This phenotype is similar to what we observed in our initial infection of cells with
310 UVM-1927 (our H3N2 subtype), where depletion of Rab11B alone blocked viral protein
311 production but simultaneous depletion of Rab11A + Rab11B rescued the phenotype (Figure
312 2E, S3). While Rab11A and Rab11B share a high degree of sequence similarity, the crystal
313 structures of the two isoforms reveal potentially significant differences, as Rab11A is seen
314 as a dimer in the crystal structure, while Rab11B crystallized as a monomer[50]. In addition,

315 there were significant differences in the confirmation of the Switch I region, which is of
316 particular interest given the likely role Rab11A's Switch I region plays in binding to PB2[30,50].
317 While it seems clear that Rab11A and Rab11B can transport distinct pools of
318 proteins to the plasma membrane, the fact that Rab11B traffics a protein (or proteins) that
319 is required for binding of H3N2 but not H1N1 subtypes of influenza virions is particularly
320 interesting given our current understanding of influenza entry. Conventional thinking of
321 influenza entry typically posits that influenza virions 'roll' along the cellular surface,
322 interacting with sialoglycans present on various glycoproteins and glycolipids which
323 mediates the first step, 'attachment'. After this binding event, more recent work proposes
324 that glycan-binding is followed by secondary engagement of the receptor, followed by
325 internalization[18]. Within this framework, it has long been recognized that the linkage type
326 and subsequent 'shape' of sialic acid modifications play important roles in the ability of a
327 given HA to bind to a particular host cell, with α2,6 linked structures forming an 'umbrella'
328 like structure preferred by human IAVs while α2,3 linkages form a 'cone' like shape that is
329 preferentially recognized by strains of avian origin[51–58].
330 Importantly, further modifications to the glycan also affect glycan topology, and it is
331 known that not every glycan with a α2,6 linkage is recognized by every influenza strain that
332 possess α2,6 receptor specificity[18]. While some studies report relatively similar glycan
333 usage between seasonal H1N1 and H3N2 isolates, H3N2 isolates often bind a smaller
334 subset of glycans[58,59]. H3N2 isolates are known to be particularly sensitive to passage in
335 eggs, with H3N2 isolates developing increased specificity for α2,6 linkages, which has
336 posed a problem for egg-grown vaccine development[60]. In addition, there are non-sialic
337 acid attachment factors that can affect HA binding, such as phosphorylated but non-
338 sialylated glycans[61]. The H17N10 and H18N11 influenza subtypes (found in South and
339 Central American bats) cannot bind sialic acid[62–64] and instead used the MHC-II receptor[65].
340 Furthermore, H2N2 viruses from both human and avian origin have dual receptor
341 specificity and are able to utilize either a sialic-acid dependent or a sialic acid-
342 independent, but MHC-II dependent, mechanism of entry[66].

343 Some studies have also shown that specific cell surface proteins have the ability to
344 interact with HA in a sialic acid-independent manner, including nucleolin[67] and natural
345 killer (NK) cell p46-related protein (NKP46)[68–70]. Other work concludes that a specific
346 sialyated protein is responsible for HA binding and subsequent internalization, with the
347 voltage-dependent CA^{2+} channel $Ca_v1.2$ reported to play this role for PR8[8]. Engagement of
348 cellular signaling receptors, including phosphatidylinositol-3-kinase and receptor tyrosine
349 kinases (RTKs) including the epidermal growth factor receptor (EGFR) have also been
350 shown to play a role in transmitting signals across the plasma membrane that lead to
351 internalization[9–14]. Finally, there are reports of subtype specific dependence on cellular
352 entry factors, with post-binding internalization of H1N1 but not H3N2 subtypes depending
353 on the phospholipase C-γ1 (PLC-γ1) signaling mediator downstream of receptor tyrosine
354 kinase pathways[15]. As much prior work has focused on binding and entry of H1N1 strains
355 (typically using the highly lab adapted PR8 strain), it is likely that further subtype
356 specificities in cellular binding and internalization receptors remain to be identified.
357 Our data clearly establishes the subtype specific role of Rab11B in the binding of
358 recent seasonal H3N2 but not H1N1 isolates. However, as Rab11B is not a transmembrane
359 protein, it almost certainly plays an indirect role in this process by trafficking a protein or
360 proteins required for H3 binding to the cell surface. Given the abundance of proteins in the
361 surface proteome with an α2,6 linkage, it seems somewhat unlikely that Rab11B is solely
362 responsible for trafficking the entire variety of proteins conventionally thought to serve as
363 the binding receptor for human IAV strains. Further arguing against a scenario in which the
364 loss of Rab11B is simply reducing cell surface levels of sialydated proteins is the fact that
365 entry and binding of H1N1 isolates from the same time period are unaffected by the
366 Rab11B depletion. Our data therefore supports the existence of a more specific protein-
367 based binding-receptor that is differentially used by H3N2 isolates from recent years
368 (Figure 9). Open questions that remain the subject of future study include determining
369 whether the Rab11B-dependent cargo that is transported to the surface is responsible for
370 mediating internalization of the virion in addition to binding. Mapping the plasma
371 membrane resident cargos of the Rab11B-dependent recycling pathway could provide a

372 valuable starting point in identifying putative attachment and/or internalization receptors
373 used specifically by recent H3N2 IAVs. Future work is also needed to determine whether
374 these findings extend to older H3N2 isolates, as well as whether this observation is true in
375 cell types of other origins and species. In summary, this work extends the well-established
376 dependence of IAV on Rab11a late in infection to include recent seasonal H1N1 and H3N2
377 isolates, while also extending our understanding of the critical role this protein family plays
378 to include Rab11b mediated binding and entry of H3N2 viruses.
379

380 **MATERIALS AND METHODS**

381 **Ethics Statement and Institutional Approvals.**

382 Research conducted in this study was reviewed and approved by the Institutional
383 Biosafety Committee of the University of Vermont (REG202100008). The use of deidentified
384 positive clinical specimens was approved by the University of Vermont Institutional Review
385 Board (STUDY00000881) under a waiver of consent.

386 **Cells.**

387 Human adenocarcinoma 549 cells (A549) (kindly obtained from Dr. Steve Baker),
388 human embryonic kidney cells (HEK-293T/17) (kindly provided by Dr. John Salogiannis),
389 human papillary adenocarcinoma lung cells, considered 'club-like cell' (NCI-H441, ATCC
390 HTB-174) and Madeline Darby Kidney cells modified to express α2,6 sialic acid and
391 TMPRSS2[71] (MDCK-SIATT) (kindly provided by Dr. Jesse Bloom via Dr. Steve Baker) were
392 cultured in 1X DMEM (Corning #06923002) with 10% FBS (Gibco #16140-071) and 1X
393 pen/strep (Corning #30-002-CI). NCI-H441 cells stably transduced with Rab11B targeting
394 shRNA were maintained in media as above, plus 3 μg/mL puromycin.

395 **Viruses.**

396 A/Burlington/UVM-1927/2022 (H3N2) (UVM-1927) and A/Burlington/UVM-0478/2022
397 (H1N1) (UVM-0478) viruses were isolated from IAV positive clinical specimens graciously
398 provided by Dr. Jessica Crothers at the University of Vermont. MDCK-SIATT cells were
399 seeded in a 12-well plate (CytoOne #CC7682-7512) at a density of 3.5×10^5 cells per well 24
400 hrs before isolation. Day of isolation, each clinical sample was brought up to a total volume

401 of 400ul in serum-free media (Corning #10-017-CM). Plated cells were washed twice in PBS
402 (Corning #21-040-CV) and 400ul of sample placed in each well. Cells were incubated for
403 1hr at 37°C and 5% CO_2, rocking the plates every 20 mins during the incubation. After 1hr,
404 the supernatants were removed from each well and replaced with 1mL media comprised of
405 Opti-MEM (Gibco #11-058-021) + 1ug/mL TPCK-Trypsin (Sigma-Aldrich #T88002-100MG) +
406 1X pen/strep (Corning #30-002-CI). Samples were deemed ready to be collected when
407 visible cytopathic effect (CPE) could be seen. At that time, supernatants were clarified at
408 10,000G for 5 minutes, transferred to clean tubes and stored at -80°C for later stock
409 generation. Low passage stock of A/Baltimore/JH-0586/2022 (H3N2) (JH-0586) virus
410 (EPI_ISL_16766241) originally isolated in human nasal epithelial cells was a kind gift of Dr.
411 Andrew Pekosz at Johns Hopkins University. A/Puerto Rico/8/1934 (H1N1) was derived by
412 reverse genetics.

413 **Generation of 7+1 Reassortants by Reverse Genetics.**

414 Viruses containing the HA or NA segments of A/Burlington/UVM-1927/2022 (H3N2)
415 in a A/Puerto Rico/8/1934 (H1N1) backbone were created by reverse genetics, using a
416 pHW2000 plasmid system kindly provided by Dr. Stacey Schultz-Cherry. The HA or NA
417 coding sequence (based on sequencing of the UVM-1927 stock) was synthesized and
418 cloned into the pHW2000 HA or NA segment plasmid (replacing the original PR8 coding
419 sequence) by Genscript. HEK-293T cells were seeded in six well plates ($7x10^5$ cells/well) in
420 complete DMEM. The following day cells were transfected with 450ng of each of the eight
421 pHW2000 plasmids (PB1, PB2, PA, HA, NP, NA, M, NS) using jetOPTIMUS (for per reaction
422 volumes of 3.5 ug combined segment DNA, 50 ul jetOPTIMUS buffer, 3.5 ul jetOPTIMUS,
423 incubated for ten minutes before dropwise addition to adherent HEK-293T cells). 24 hours
424 post transfection media was removed and HEK 293T cells were overlaid with $3x10^5$ MDCK-
425 SIATT cells/well resuspended in 2 ml OPTI-VGM (optiMEM, 0.19% BSA, 1X Pen/Strep, 1
426 ug/ml TPCK Trypsin). Cells were monitored every 24 hr for cytopathic effect compared to a
427 transfection control lacking PB2. Once CPE was observed, rescued virus was blind
428 passaged by infecting a confluent T25 of MDCK-SIATT cells with 500 ul clarified rescue

429 supernatant combined with 500 ul OPTI-VGM, 2 ug/ml TPCK-trypsin for three days. Blind
430 passages were titered by plaque assay and used to generate additional high titer stocks.

431 **Viral Stocks.**

432 Viral stocks were grown by seeding 4.2 x 10^6 cells/flask of MDCK-SIATTs in a T150
433 flask (Corning #430825) in 1X DMEM (Corning #06923002) with 10% FBS (Gibco #16140-
434 071) and 1X pen/strep (Corning #30-002-CI) and incubated overnight at 37°C and 5% CO_2.
435 Each flask was washed twice with PBS (Corning #21-040-CV) to remove serum and
436 infected at an MOI of 0.001 in a volume of 5 ml for one hour, overlaid with 15 ml of Opti-
437 MEM (Gibco #11058-021) plus 1 ug/ml TPCK trypsin (Sigma-Aldrich #T88002-100MG) and
438 incubated at 37°C until ~50% CPE was observed.

439 **Viral Infections.**

440 Viral infections were performed at the indicated MOI, by first washing the cells once
441 with PBS (Corning #21-040-CV) and then infecting with an inoculum made up of virus plus
442 1X DMEM (Corning #06923002) at 37°C and 5% CO_2 for one hour. Cells were rocked every
443 20 minutes, and after one hour the inoculum was removed and replaced with an overlay of
444 Opti-MEM (Gibco #11058-021) before incubating for the indicated time at 37°C. Viral
445 supernatants were clarified by centrifuging at 10,000G for 5 minutes to remove any cell
446 debris, aliquoted into two separate tubes and stored at -80°C.

447 **Viral Plaque Assays.**

448 Infectious viral production was assessed using plaque assays. MDCK-SIATT cells
449 were trypsinized using 0.25% trypsin-EDTA (Gibco #25200-0720) for 10-15 minutes and
450 seeded at 1x10^6 cells/well of a six well plate (Corning #3506) The following day wells were
451 washed with PBS (Corning #21-040-CV) or DMEM (Corning #06923002) and inoculated with
452 serial ten-fold dilutions of each sample in DMEM. After infection, cells were placed at 37°C
453 with 5% CO_2 for an hour and rocked every 15 minutes to ensure even mixing and prevent
454 cell death from drying. After one hour, cells were overlayed with 2 ml of a warmed 1:1
455 mixture of 2.4% Avicel RC-591 NF (Dupont #RC591-NFDR080) + 1X DMEM (Corning
456 #06923002) + 1 ug/ml TPCK trypsin (Sigma-Aldrich #T88002-100MG). Cells were returned
457 to 37°C for 48 hours, and care was taken not to disturb the plates during this period. Finally,

458 cells were washed with PBS (Corning #21-040-CV), fixed with 4% formaldehyde (Honeywell
459 #F16354L) for 20 minutes and stained with 0.1% crystal violet (Fisher #C581-100) for five
460 minutes. Plates were rinsed three times with water and allowed to dry before plaques were
461 counted to determine viral titer.

462 **Viral Sequencing.**

463 Viral subtypes were identified through amplicon based whole genome sequencing.
464 In brief, RNA from viral stocks was extracted using a QIAamp Viral RNA Mini Kit (Qiagen
465 #52906) according to manufacturer's protocols, and one step RT-PCR was used to amplify
466 all eight segments using universal primers[72] and Superscript III high-fidelity RT-PCR kit
467 (Invitrogen #12574-035).

Sequencing Primers (RT-PCR)		
Name/Target	**Company, Catalog #**	**Sequence**
Uni12/Inf-1_IAV[72]	IDT	5'-GGGGGGAGCAAAAGCAGG-3'
Uni12/Inf-3_IAV[72]	IDT	5'-GGGGGGAGC**G**AAAGCAGG-3'
Uni13/Inf-1_IAV[72]	IDT	5'-CGGGTTATTAGTAGAAACAAGG-3'

468 Per reaction, 8.75 ul nuclease free water, 12.5 ul of 2X RT-PCR buffer 0.2 ul of 10 uM
469 Uni12/Inf-1, 0.3 ul of 10 uM Uni12/Inf-3, 0.5 uL of 10 uM Uni13/Inf-1, and 0.25 ul RT/Taq
470 enzyme mix were combined with 2.5 ul of RNA template. RT-PCR was run on a Eppendorf
471 Mastercycler Nexus Thermal Cycler with the following cycling conditions: 55°C/2 min,
472 45°C/60 min, 94°C/2 min, 5 cycles of [94°C/30s; 44°C/30s; 68°C/3.5 min], 26 cycles of
473 [94°C/30s; 57°C/30s; 68°C/3.5 min], 68°C/10 min, hold at 4°C.

474 Successful amplification was confirmed by visualizing PCR products (i.e., seven-
475 eight bands) on a 1% agarose (Fisher #BP160-500) gel for 2 hours at 120V. Samples were
476 then purified using a QIAquick PCR Purification Kit (Qiagen #28104) and Illumina based
477 amplicon sequencing conducted by the Emory EPC Genomics Core.

478 We used a Nextflow pipeline developed by Dr. Ramiro Barrantes Reynolds at the
479 Vermont Integrative Genomics Resource Core. This pipeline uses Nextflow/NF-Core based
480 UPHL-BioNGS/Walkercreek v2.0.0 bioinformatics pipeline for analysis and adds a custom
481 Nextflow pipeline for generating a phylogenetic tree[73–79]. We compared the similarity
482 between our two H3N2s by using an RShiny app developed to examine the results of the

483 pipeline described above and understand the sequence level differences between the two
484 viruses. We identified their relatedness through the tree created by the pipeline described
485 above[80]. All R coding was done in RStudio[81] (R2023.09.1+494) and we used Nextflow
486 24.04.4 for pipeline development. Computation was done using the Vermont Advanced
487 Computing Center (VACC).

488 **siRNA knockdowns.**

489 A549 cells were seeded in 24 well plates at a density of $1.5x10^5$ cells/well, in a
490 volume of 500 ul. Transfections were performed on cells in suspension or within 24 hours
491 of plating. To knockdown our gene of interest, we transiently transfected siRNA sequence
492 targeting Rab11A, Rab11B, Rab11A+B, Rab8A or a non-targeting siRNA, using
493 Lipofectamine RNAiMAX Reagent (Invitrogen #56532) in A549 cells. For each well, we
494 combined 1.2 uL of 10 uM siRNA stock with 198.6 ul of Opti-MEM (Gibco #11058-021) and
495 2 ul of RNAiMax (Invitrogen #56532), gently mixed and allowed to rest for 20 minutes before
496 adding to cells dropwise. 48 hours post transfection cells were either infected, or RNA was
497 harvested to verify mRNA knockdown at the time of infection.

siRNA Target	Company, Catalog #	Assay ID
Non-targeting control	ThermoFisher, 4390843	NA
Rab11A	ThermoFisher, 4390824	s16704
Rab11B	ThermoFisher, 4390824	s17648
Rab8A	ThermoFisher, 4390824	s8681

498

499 **shRNA depletion**

500 **Lentivirus Generation:** A custom lentiviral construct driving inducible shRNA
501 expression targeting human Rab11B was obtained from Horizon Discovery (SMARTvector
502 inducible human Rab11B mCMV-Turbo RFP shRNA). Lentiviral particles were generated by
503 transfecting subconfluent HEK-293T cells with 6 ug of the Rab11B SMARTvector construct
504 and 28.5 ug of the Horizon Trans-Lentiviral shRNA packaging kit (Horizon Discovery, cat #
505 TLP5912) using jetOPTIMUS (Sartorius Item # 101000025) according to the manufacturer's
506 instructions. Cells were incubated for 16 hrs before transfection media was changed to
507 reduced serum media (1X DMEM containing 5% FBS, 1X Pen/Strep). For each of the

508 following three days, supernatant was collected and replaced with fresh media. The
509 supernatants were clarified and stored at -80°C for use in subsequent transductions.
510 **Lentiviral transduction:** H441 cells were seeded at $1.5x10^5$ cells/well in a 24 well
511 plate and transduced the following day with lentiviral supernatants by spinnoculation.
512 H441 cells were inoculated with 500 ul total volume (consisting of complete DMEM, 0.5 µl
513 polybrene, and 100µl of lentiviral supernatant). Cells were spun for two hours at 640xG,
514 20°C, after which cells were returned to the incubator. The following day, media was
515 replaced, and cells were returned to the incubator. Three days post transduction cells were
516 selected with puromycin (3 µg/mL), the dilution in which ~30% of cells survived was
517 maintained in puromycin containing media and expanded for future use.
518 **Silencing and validation:** Rab11B depletion was optimized by comparing a range of
519 doxycycline concentrations (0.1 µg, 0.5 µg, 2 µg, 4 µg) and times post induction (24, 48, 72
520 hrs). Rab11B silencing was measured by RT-qPCR, cells were lysed in 350 µl of RLT buffer
521 for RNA extraction and RT-qPCR as described below. The optimal time and concentration
522 was found to be 4 ug/mL of doxycycline 72 hrs post induction so this was used for all
523 further shRNA depletion experiments.
524 **RNA extraction.**
525 48 hrs after transfection, cells treated with siRNAs were lysed in 350 ul of RLT lysis
526 buffer (from RNeasy Mini Kit). Cell lysates were processed, and RNA was extracted using
527 the QIAshredder columns (Qiagen #79656) followed by RNeasy Mini Kit (Qiagen #74106)
528 coupled with on column DNase treatment using RNase-Free DNase Set (Qiagen #79256),
529 according to manufacturer's protocols.
530 **RT-qPCR.**
531 We used a 20 ul reaction consisting of 5 ul of New England Biolabs Luna Probe One-
532 Step RT-qPCR 4X Mix with UDG (NEB #M3019E), 1 ul of the 20X primer/probes stock, 1 ul of
533 extracted RNA, and 13 ul of nuclease-free water for all of our RT-qPCR with pre-mixed
534 primer/probes (listed below). To measure levels of IAV, we used the SVIP-MPv2 primers and
535 probe[82]. We again used 20 ul reaction volume with 5 ul of New England Biolabs Luna Probe
536 One-Step RT-qPCR 4X Mix with UDG (NEB #M3019E), 0.28 ul each of 100 uM forward and

537 reverse primer stock, 0.08 ul of 100 uM probe stock, 13.36 ul of nuclease-free water, and 1
538 ul of template RNA. Each sample was run in triplicate, and each primer/probe set had a no
539 template control. Once loaded into plates (Applied Biosystems #4306737), samples were
540 spun at 400 g for 5 minutes. RT-qPCR was run using a QuantStudio Real-Time PCR system
541 using the following cycling conditions: 55°C/10 min, 95°C/1 min, 45 cycles of [95°C/10s;
542 60°C/30s], 4°C hold. Relative RNA levels were determined using the $\Delta\Delta C_T$ method, using
543 18S RNA levels as the housekeeping control.
544

RT-qPCR Primers		
Target	**Company, Catalog #**	**Assay ID/Sequence**
18S	ThermoFisher, #4331182	Hs99999901_s1
Rab11A	ThermoFisher, #4331182	Hs00366449_g1
Rab11B	ThermoFisher, #4331182	Hs00188448_m1
Rab8A	ThermoFisher, #4331182	Hs00180479_m1
SVIP-MPv2[82]	IDT	F: 5'-GGCCCCCTCAAAGCCGA-3' R: 5'-CGTCTACGYTGCAGTCC-3' P2-MGB: 5'-TCACTKGGCACGGTGAGCGT-3' (Label: 5'-FAM-3'MGB-NFQ(EQ))

545

546 **Antibodies.**

Primary Antibodies		
Species, Target	**Company, Catalog #**	**Dilution Used**
Rabbit anti-HA	Sino Biological #86001-RM01	1:5,000 (western blot) 1:1,000 (flow cytometry)
Mouse anti-M2 (14C2)	Abcam #AB5416-1001	1:5,000 (western blot) 1:1,000 (flow cytometry)
Mouse anti-NP (HB65)	BioXCell #BE0159R001MG	1:1000 (western blot)
Anti-GAPDH	Abcam #AB181602	1:10,000 (western blot)
Rabbit anti-Udorn (H3N2)	From Dr. Robert Lamb	1:1,000 (flow cytometry)
Secondary Antibodies		
IRDye 680LT goat anti-rabbit IgG	LICOR #92668021	1:10,000
IRDye 680RD goat anti-mouse IgG	LICOR #92668070	1:10,000
IRDye 800CW goat anti-mouse IgG	LICOR #92632210	1:10,000
Alexa Fluor 488 anti-rabbit	Invitrogen #A11034	1:1,000
Alexa Fluor 647 anti-mouse	Invitrogen #2555690	1:1,000

547

548 **Protein analysis.**

549 Samples were prepared for protein analysis and western blot largely as previously
550 published (Kubinski, 2024). Briefly, cells were lysed in a NP-40 (Alfa Asear #J60766) + 1%
551 Triton X-100 (Fisher #BP151-100) supplemented with Pierce Protease Inhibitor Mini Tablets
552 (Thermo Scientific #A32955) for 20 mins on ice. Cell lysates were clarified, then diluted 1:1
553 (v/v) with 4X Laemmli sample buffer (250 mM Tris-HCl pH 6.8, 40% glycerol, 8% SDS,
554 0.04% Bromophenol Blue, 2.75mM 2-mercaptoethanol). All samples were heated to 95°C
555 for 5-10 mins before loading. Samples were separated in NuPAGE 4–12% Bis-Tris gels
556 (Invitrogen # NPO335BOX) in MES buffer (Invitrogen # NP0002) with a molecular mass
557 ladder (Thermo Fisher #LC5925) at 180v for 50 mins before being transferred into a
558 nitrocellulose membrane (Invitrogen # IB23001) using an iBlot 2 machine (Invitrogen) at 20V
559 for seven minutes.

560 Membranes were blocked in a 5% milk/PBS solution for 30 minutes and then
561 incubated overnight at 4°C in a solution containing the primary antibody in a 5% milk/PBST
562 (PBS + 0.2% Tween 20). Membranes were washed three by five minutes in PBST, incubated
563 while rocking with secondary antibodies diluted in 5% milk/PBST for 45 minutes, washed
564 again with PBST and imaged with a LI-COR Odyssey CLx. Protein expression was analyzed
565 by measuring band densitometry in the LI-COR software package, Image Studio (Ver 5.5).

566 **Flow Cytometry**

567 Infected cells were washed in PBS, trypsinized, and fixed in a final concentration of 4%
568 paraformaldehyde (Thermo Scientific #043368.9M) for 20 minutes. After fixing, cells were
569 transferred to 5 mL polystyrene round-bottom tubes (Falcon #352052) and spun at 400g for
570 5 minutes to pellet cells. Supernatants were discarded and cells resuspended in 4 mL of
571 wash buffer (1X PBS/5% FBS). Cells were pelleted and 200 ul of PBS/0.05% Triton X-100
572 (Fisher #BP151-100) solution was added to permeabilize for five minutes. Cells were
573 pelleted and washed as above before resuspending in 1 mL of wash buffer for one hour to
574 block. Cells were pelleted and resuspended in 200 ul of primary antibody solution (diluted
575 in wash buffer) for one hour. Cells were pelleted and washed as above before resuspension
576 in 200 ul of secondary antibody solution (again diluted in wash buffer) for one hour

577 (protected from light). Cells were washed and pelleted one final time after which they were
578 resuspended in 200 ul of sterile PBS and stored at 4°C protected from light until flow
579 cytometry was performed. Samples were run on a Beckman CytoFlex (2L/4 flourescences)
580 in the Harry Hood Bassett Flow Cytometry and Small Particles Detection facility
581 (RRID:SCR_022147) at the UVM-LCOM and analyzed using FloJo software (v10.10.0).

582 **Binding Assay**

583 Cells that had been transfected with siRNA 48 hrs earlier were placed on ice to cool,
584 washed with ice cold PBS and infected with virus at an MOI of 1 (diluted in a binding buffer
585 of Opti-MEM, 10 mM HEPES,10 mM MES to prevent changes in pH during incubation
586 without CO_2). Cells remained on ice (to prevent endocytosis), virus was bound for one hour
587 and rocked every 15 mins to ensure cells an equal distribution of viral inoculum and
588 prevent cells from drying. Cells were then washed three times with ice cold PBS to remove
589 unbound virions. At this point, cells were either lysed in 350 ul RLT buffer (for RNA
590 extraction and analysis of bound virions) or used for the time of addition assay.
591 Alternatively, cells were treated with 0.0043 U/ul of exogenous neuraminidase (Roche
592 #11585886001) for 20 minutes at 37°C to strip bound virions from the cell surface[21]. Cells
593 were washed three times with PBS after neuraminidase treatment before lysis in 350 ul RLT
594 as above.

595 **Time of Addition**

596 Using a protocol adapted from one recently described by the Chlanda lab [44], we first
597 synchronized infection using the binding protocol described above. After the initial hour of
598 viral binding, cells were overlaid with Opti-MEM and were placed at 37°C. At 0, 20, 45, 60,
599 or 90 mins, the Opti-MEM was removed and replaced with Opti-MEM containing 15 mM
600 ammonium chloride (NH_4Cl). Cells were then incubated at 37°C for 16 hrs, before
601 preparing for flow cytometry as described above.

602

603 **Acknowledgements**

604 We would like to thank Drs Edward Hutchinson, Margaret Kielian, Chris Huston,
605 John Salogiannis, and Bruno Martorelli Di Genova for helpful discussion, Dr. Stacey

Schultz-Cherry for the PR8 reverse genetics system, and Dr Andrew Pekosz for providing the A/Baltimore/JH-0586 (H3N2) viral isolate. All flow cytometric (small particle detection) data were carried out in the Harry Hood Bassett Flow Cytometry and Small Particles Detection facility (RRID:SCR_022147) at the UVM-LCOM and we thank Dr. Roxana del Rio-Guerra for her technical assistance with flow cytometry. The authors acknowledge the Vermont Advanced Computing Center (VACC) at the University of Vermont for providing computational resources that have contributed to the research results reported within this paper.

Funding

This study was supported by the Microbiology and Molecular Genetics Department 2024 Distinguished Undergraduate Research Summer Award (A.H.T.), NIH K23AI175660 (J.W.C.), NIH (NIGMS) award P20GM125498 (E.A.B) and UVM start-up funds (E.A.B.).

Data Availability

Raw sequencing data are available in the NCBI Bioproject ID PRJNA1254704.

REFERENCES

1. Influenza (seasonal). https://www.who.int/news-room/fact-sheets/detail/influenza-(seasonal).
2. CDC. First H5 Bird Flu Death Reported in United States. *CDC Newsroom* https://www.cdc.gov/media/releases/2025/m0106-h5-birdflu-death.html (2025).
3. Hutchinson, E. C. & Yamauchi, Y. Understanding Influenza. in *Methods in Molecular Biology* 1–21 (Springer New York, 2018). doi:10.1007/978-1-4939-8678-1_1.
4. Krammer, F. *et al*. Influenza. *Nat Rev Dis Primers* **4**, 1–21 (2018).
5. Dourmashkin, R. R. & Tyrrell, D. A. J. Electron Microscopic Observations on the Entry of Influenza Virus into Susceptible Cells. *Journal of General Virology* **24**, 129–141 (1974).
6. Gottschalk, A. On the Mechanism Underlying Initiation of Influenza Virus Infection. in *Ergebnisse der Mikrobiologie Immunitätsforschung und Experimentellen Therapie* (eds Kikuth, W., Meyer, K. F., Nauck, E. G., Pappenheimer, A. M. & Tomcsik, J.) 1–22 (Springer Berlin Heidelberg, Berlin, Heidelberg, 1959).
7. Luo, M. Influenza Virus Entry. in *Viral Molecular Machines* (eds Rossmann, M. G. & Rao, V. B.) 201–221 (Springer US, Boston, MA, 2012). doi:10.1007/978-1-4614-0980-9_9.
8. Fujioka, Y. *et al*. A Sialylated Voltage-Dependent Ca2+ Channel Binds Hemagglutinin and Mediates Influenza A Virus Entry into Mammalian Cells. *Cell Host & Microbe* **23**, 809-818.e5 (2018).
9. Eierhoff, T., Hrincius, E. R., Rescher, U., Ludwig, S. & Ehrhardt, C. The epidermal growth factor receptor (EGFR) promotes uptake of influenza A viruses (IAV) into host cells. *PLoS Pathog* **6**, e1001099 (2010).

644 10. Hale, B. G., Jackson, D., Chen, Y.-H., Lamb, R. A. & Randall, R. E. Influenza A virus NS1
645 protein binds p85β and activates phosphatidylinositol-3-kinase signaling. *Proceedings*
646 *of the National Academy of Sciences* **103**, 14194–14199 (2006).
647 11. Kumar, N., Liang, Y., Parslow, T. G. & Liang, Y. Receptor Tyrosine Kinase Inhibitors Block
648 Multiple Steps of Influenza A Virus Replication. *Journal of Virology* **85**, 2818–2827
649 (2011).
650 12. Kumar, N., Sharma, N. R., Ly, H., Parslow, T. G. & Liang, Y. Receptor Tyrosine Kinase
651 Inhibitors That Block Replication of Influenza A and Other Viruses. *Antimicrobial Agents*
652 *and Chemotherapy* **55**, 5553–5559 (2011).
653 13. Pleschka, S. *et al.* Influenza virus propagation is impaired by inhibition of the
654 Raf/MEK/ERK signalling cascade. *Nat Cell Biol* **3**, 301–305 (2001).
655 14. Sieben, C., Sezgin, E., Eggeling, C. & Manley, S. Influenza A viruses use multivalent
656 sialic acid clusters for cell binding and receptor activation. *PLOS Pathogens* **16**,
657 e1008656 (2020).
658 15. Zhu, L., Ly, H. & Liang, Y. PLC-γ1 signaling plays a subtype-specific role in postbinding
659 cell entry of influenza A virus. *J Virol* **88**, 417–424 (2014).
660 16. Peng, W. *et al.* Recent H3N2 Viruses Have Evolved Specificity for Extended, Branched
661 Human-type Receptors, Conferring Potential for Increased Avidity. *Cell Host & Microbe*
662 **21**, 23–34 (2017).
663 17. Lin, Y. P. *et al.* Evolution of the receptor binding properties of the influenza A(H3N2)
664 hemagglutinin. *Proceedings of the National Academy of Sciences* **109**, 21474–21479
665 (2012).

666 18. Karakus, U., Pohl, M. O. & Stertz, S. Breaking the Convention: Sialoglycan Variants,
667 Coreceptors, and Alternative Receptors for Influenza A Virus Entry. *Journal of Virology*
668 **94**, 10.1128/jvi.01357-19 (2020).
669 19. Sempere Borau, M. & Stertz, S. Entry of influenza A virus into host cells - recent
670 progress and remaining challenges. *Curr Opin Virol* **48**, 23–29 (2021).
671 20. Daniels, R. S., Douglas, A. R., Skehel, J. J. & Wiley, D. C. Analyses of the Antigenicity of
672 Influenza Haemagglutinin at the pH Optimum for Virus-mediated Membrane Fusion.
673 *Journal of General Virology* **64**, 1657–1662 (1983).
674 21. Matlin, K. S., Reggio, H., Helenius, A. & Simons, K. Infectious entry pathway of influenza
675 virus in a canine kidney cell line. *Journal of Cell Biology* **91**, 601–613 (1981).
676 22. Skehel, J. J. & Wiley, D. C. Receptor Binding and Membrane Fusion in Virus Entry: The
677 Influenza Hemagglutinin. *Annual Review of Biochemistry* **69**, 531–569 (2000).
678 23. White, J., Kartenbeck, J. & Helenius, A. Membrane fusion activity of influenza virus. *The*
679 *EMBO Journal* **1**, 217–222 (1982).
680 24. Helenius, A. Unpacking the incoming influenza virus. *Cell* **69**, 577–578 (1992).
681 25. Hutchinson, E. C. & Fodor, E. Transport of the Influenza Virus Genome from Nucleus to
682 Nucleus. *Viruses* **5**, 2424–2446 (2013).
683 26. Amorim, M. J. *et al.* A Rab11- and Microtubule-Dependent Mechanism for Cytoplasmic
684 Transport of Influenza A Virus Viral RNA. *Journal of Virology* **85**, 4143–4156 (2011).
685 27. Eisfeld, A. J., Kawakami, E., Watanabe, T., Neumann, G. & Kawaoka, Y. RAB11A Is
686 Essential for Transport of the Influenza Virus Genome to the Plasma Membrane. *Journal*
687 *of Virology* **85**, 6117–6126 (2011).

688 28. Momose, F. *et al.* Apical Transport of Influenza A Virus Ribonucleoprotein Requires
689 Rab11-positive Recycling Endosome. *PLOS ONE* **6**, e21123 (2011).
690 29. Stenmark, H. Rab GTPases as coordinators of vesicle traffic. *Nat Rev Mol Cell Biol* **10**,
691 513–525 (2009).
692 30. Veler, H. *et al.* The C-Terminal Domains of the PB2 Subunit of the Influenza A Virus RNA
693 Polymerase Directly Interact with Cellular GTPase Rab11a. *Journal of Virology* **96**,
694 e01979-21 (2022).
695 31. Bhagwat, A. R. *et al.* Quantitative live cell imaging reveals influenza virus manipulation
696 of Rab11A transport through reduced dynein association. *Nat Commun* **11**, 23 (2020).
697 32. de Castro Martin, I. F. *et al.* Influenza virus genome reaches the plasma membrane via a
698 modified endoplasmic reticulum and Rab11-dependent vesicles. *Nat Commun* **8**, 1396
699 (2017).
700 33. Vale-Costa, S. *et al.* Influenza A virus ribonucleoproteins modulate host recycling by
701 competing with Rab11 effectors. *Journal of Cell Science* **129**, 1697–1710 (2016).
702 34. Han, J. *et al.* Host factor Rab11a is critical for efficient assembly of influenza A virus
703 genomic segments. *PLOS Pathogens* **17**, e1009517 (2021).
704 35. Vale-Costa, S. *et al.* ATG9A regulates the dissociation of recycling endosomes from
705 microtubules to form liquid influenza A virus inclusions. *PLOS Biology* **21**, e3002290
706 (2023).
707 36. Vale-Costa, S. & and Amorim, M. J. Clustering of Rab11 vesicles in influenza A virus
708 infected cells creates hotspots containing the 8 viral ribonucleoproteins. *Small*
709 *GTPases* **8**, 71–77 (2017).

710 37. Nturibi, E., Bhagwat, A. R., Coburn, S., Myerburg, M. M. & Lakdawala, S. S. Intracellular
711 Colocalization of Influenza Viral RNA and Rab11A Is Dependent upon Microtubule
712 Filaments. *J Virol* **91**, e01179-17 (2017).
713 38. Lakdawala, S. S. *et al.* Influenza A Virus Assembly Intermediates Fuse in the
714 Cytoplasm. *PLoS Pathog* **10**, e1003971 (2014).
715 39. Chou, Y. *et al.* Colocalization of Different Influenza Viral RNA Segments in the
716 Cytoplasm before Viral Budding as Shown by Single-molecule Sensitivity FISH Analysis.
717 *PLOS Pathogens* **9**, e1003358 (2013).
718 40. Ganti, K., Han, J., Manicassamy, B. & Lowen, A. C. Rab11a mediates cell-cell spread
719 and reassortment of influenza A virus genomes via tunneling nanotubes. *PLoS Pathog*
720 **17**, e1009321 (2021).
721 41. Bruce, E. A., Digard, P. & Stuart, A. D. The Rab11 pathway is required for influenza A
722 virus budding and filament formation. *J Virol* **84**, 5848–5859 (2010).
723 42. Ferro, E., Bosia, C. & Campa, C. C. RAB11-Mediated Trafficking and Human Cancers:
724 An Updated Review. *Biology (Basel)* **10**, 26 (2021).
725 43. Grimsey, N. J., Coronel, L. J., Cordova, I. C. & Trejo, J. Recycling and Endosomal Sorting
726 of Protease-activated Receptor-1 Is Distinctly Regulated by Rab11A and Rab11B
727 Proteins*. *Journal of Biological Chemistry* **291**, 2223–2236 (2016).
728 44. Peterl, S. *et al.* Morphology-dependent entry kinetics and spread of influenza A virus.
729 2024.08.01.605992 Preprint at https://doi.org/10.1101/2024.08.01.605992 (2024).
730 45. Pinto, R. M., Lycett, S., Gaunt, E. & Digard, P. Accessory Gene Products of Influenza A
731 Virus. *Cold Spring Harb Perspect Med* **11**, a038380 (2021).

732 46. Petersen, J. *et al.* The Major Cellular Sterol Regulatory Pathway Is Required for Andes
733 Virus Infection. *PLOS Pathogens* **10**, e1003911 (2014).
734 47. Kelly, E. E., Horgan, C. P. & McCaffrey, M. W. Rab11 proteins in health and disease.
735 *Biochemical Society Transactions* **40**, 1360–1367 (2012).
736 48. Haugsten, E. M., Brech, A., Liestøl, K., Norman, J. C. & Wesche, J. Photoactivation
737 Approaches Reveal a Role for Rab11 in FGFR4 Recycling and Signalling. *Traffic* **15**, 665–
738 683 (2014).
739 49. Silvis, M. R. *et al.* Rab11b Regulates the Apical Recycling of the Cystic Fibrosis
740 Transmembrane Conductance Regulator in Polarized Intestinal Epithelial Cells. *MBoC*
741 **20**, 2337–2350 (2009).
742 50. Scapin, S. M. N. *et al.* The crystal structure of the small GTPase Rab11b reveals critical
743 differences relative to the Rab11a isoform. *Journal of Structural Biology* **154**, 260–268
744 (2006).
745 51. Chandrasekaran, A. *et al.* Glycan topology determines human adaptation of avian
746 H5N1 virus hemagglutinin. *Nat Biotechnol* **26**, 107–113 (2008).
747 52. Eisen, M. B., Sabesan, S., Skehel, J. J. & Wiley, D. C. Binding of the Influenza A Virus to
748 Cell-Surface Receptors: Structures of Five Hemagglutinin–Sialyloligosaccharide
749 Complexes Determined by X-Ray Crystallography. *Virology* **232**, 19–31 (1997).
750 53. Gamblin, S. J. *et al.* The Structure and Receptor Binding Properties of the 1918 Influenza
751 Hemagglutinin. *Science* **303**, 1838–1842 (2004).

752 54. Ha, Y., Stevens, D. J., Skehel, J. J. & Wiley, D. C. X-ray structures of H5 avian and H9
753 swine influenza virus hemagglutinins bound to avian and human receptor analogs.
754 *Proceedings of the National Academy of Sciences* **98**, 11181–11186 (2001).
755 55. Ha, Y., Stevens, D. J., Skehel, J. J. & Wiley, D. C. X-ray structure of the hemagglutinin of a
756 potential H3 avian progenitor of the 1968 Hong Kong pandemic influenza virus☆.
757 *Virology* **309**, 209–218 (2003).
758 56. Rogers, G. N. & Paulson, J. C. Receptor determinants of human and animal influenza
759 virus isolates: Differences in receptor specificity of the H3 hemagglutinin based on
760 species of origin. *Virology* **127**, 361–373 (1983).
761 57. Russell, R. J. *et al.* Structure of influenza hemagglutinin in complex with an inhibitor of
762 membrane fusion. *Proceedings of the National Academy of Sciences* **105**, 17736–17741
763 (2008).
764 58. Stevens, J. *et al.* Glycan Microarray Analysis of the Hemagglutinins from Modern and
765 Pandemic Influenza Viruses Reveals Different Receptor Specificities. *Journal of*
766 *Molecular Biology* **355**, 1143–1155 (2006).
767 59. Byrd-Leotis, L. *et al.* Shotgun glycomics of pig lung identifies natural endogenous
768 receptors for influenza viruses. *Proc Natl Acad Sci U S A* **111**, E2241-2250 (2014).
769 60. Stevens, J. *et al.* Receptor specificity of influenza A H3N2 viruses isolated in
770 mammalian cells and embryonated chicken eggs. *J Virol* **84**, 8287–8299 (2010).
771 61. Byrd-Leotis, L. *et al.* Influenza binds phosphorylated glycans from human lung. *Science*
772 *Advances* **5**, eaav2554 (2019).

773 62. Sun, X. *et al.* Bat-Derived Influenza Hemagglutinin H17 Does Not Bind Canonical Avian
774 or Human Receptors and Most Likely Uses a Unique Entry Mechanism. *Cell Reports* **3**,
775 769–778 (2013).
776 63. Tong, S. *et al.* New World Bats Harbor Diverse Influenza A Viruses. *PLOS Pathogens* **9**,
777 e1003657 (2013).
778 64. Zhu, X. *et al.* Hemagglutinin homologue from H17N10 bat influenza virus exhibits
779 divergent receptor-binding and pH-dependent fusion activities. *Proceedings of the*
780 *National Academy of Sciences* **110**, 1458–1463 (2013).
781 65. Karakus, U. *et al.* MHC class II proteins mediate cross-species entry of bat influenza
782 viruses. *Nature* **567**, 109–112 (2019).
783 66. Karakus, U. *et al.* MHC class II proteins mediate sialic acid independent entry of human
784 and avian H2N2 influenza A viruses. *Nat Microbiol* **9**, 2626–2641 (2024).
785 67. Chan, C.-M. *et al.* Hemagglutinin of influenza A virus binds specifically to cell surface
786 nucleolin and plays a role in virus internalization. *Virology* **494**, 78–88 (2016).
787 68. Achdout, H. *et al.* Enhanced Recognition of Human NK Receptors After Influenza Virus
788 Infection1. *The Journal of Immunology* **171**, 915–923 (2003).
789 69. Ho, J. W. *et al.* H5-Type Influenza Virus Hemagglutinin Is Functionally Recognized by the
790 Natural Killer-Activating Receptor NKp44. *Journal of Virology* **82**, 2028–2032 (2008).
791 70. Mandelboim, O. *et al.* Recognition of haemagglutinins on virus-infected cells by NKp46
792 activates lysis by human NK cells. *Nature* **409**, 1055–1060 (2001).

71. Lee, J. M. *et al.* Deep mutational scanning of hemagglutinin helps predict evolutionary fates of human H3N2 influenza variants. *Proc Natl Acad Sci U S A* **115**, E8276–E8285 (2018).

72. Zhou, B. & Wentworth, D. E. Influenza A Virus Molecular Virology Techniques. in *Influenza Virus: Methods and Protocols* (eds Kawaoka, Y. & Neumann, G.) 175–192 (Humana Press, Totowa, NJ, 2012). doi:10.1007/978-1-61779-621-0_11.

73. Iverson, T. WalkerCreek: A Nextflow Pipeline for Influenza Genome Analysis. UPHL-BioNGS (2023).

74. Ewels, P. A. *et al.* The nf-core framework for community-curated bioinformatics pipelines. *Nat Biotechnol* **38**, 276–278 (2020).

75. Di Tommaso, P. *et al.* Nextflow enables reproducible computational workflows. *Nat Biotechnol* **35**, 316–319 (2017).

76. Katoh, K., Misawa, K., Kuma, K. & Miyata, T. MAFFT: a novel method for rapid multiple sequence alignment based on fast Fourier transform. *Nucleic Acids Research* **30**, 3059–3066 (2002).

77. Kurtzer, G. M., Sochat, V. & Bauer, M. W. Singularity: Scientific containers for mobility of compute. *PLOS ONE* **12**, e0177459 (2017).

78. Minh, B. Q. *et al.* IQ-TREE 2: New Models and Efficient Methods for Phylogenetic Inference in the Genomic Era. *Molecular Biology and Evolution* **37**, 1530–1534 (2020).

79. Shepard, S. S. *et al.* Viral deep sequencing needs an adaptive approach: IRMA, the iterative refinement meta-assembler. *BMC Genomics* **17**, 708 (2016).

80. Chang, W. shiny: Web Application Framework for R. R package version 1.12.0. (2025).

81. Posit team. *RStudio: Integrated Development Environment for R*. (Posit Software, PBC, Boston, MA, 2023).

82. Nagy, A. *et al*. A universal RT-qPCR assay for “One Health” detection of influenza A viruses. *PLOS ONE* **16**, e0244669 (2021).

Fig 1

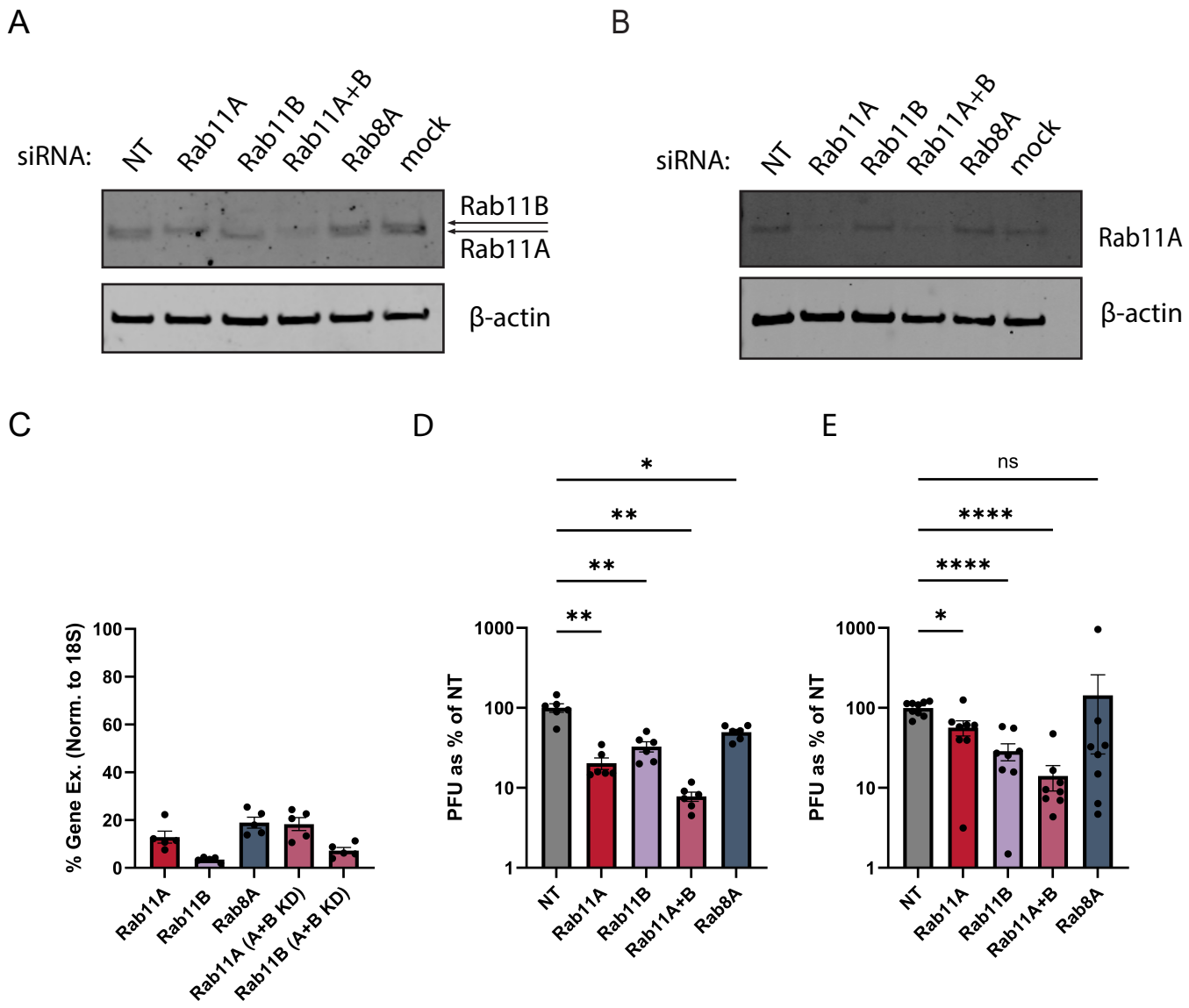
A
siRNA:
NT
Rab11A
Rab11B
Rab11A+B
Rab8A
mock
Rab11B
Rab11A
β-actin
B
siRNA:
NT
Rab11A
Rab11B
Rab11A+B
Rab8A
mock
Rab11A
β-actin
C
% Gene Ex. (Norm. to 18S)
100
80
60
40
20
0
Rab11A
Rab11B
Rab8A
Rab11A (A+B KD)
Rab11B (A+B KD)
D
*
**
**
**
PFU as % of NT
1000
100
10
1
NT
Rab11A
Rab11B
Rab11A+B
Rab8A
E
ns
****
****
*
PFU as % of NT
1000
100
10
1
NT
Rab11A
Rab11B
Rab11A+B
Rab8A

854 **Figure 1. Rab11A and Rab11B are required for replication of recent H1N1 and H3N2**
855 **influenza A isolates.**
856 A549 cells were treated with siRNAs targeting Rab11A, Rab11B (singly and in combination),
857 Rab8A or a non-targeting control. 48 hours post transfection cells were harvested to
858 determine protein (**A, B**) or RNA (**C**) expression. **A)** Total Rab11 (Rab11A plus Rab11B) or **B)**
859 Rab11A expression was detected by western blot using either non-specific or Rab11A
860 specific isoform antibodies. **C)** Relative gene expression was determined by RT-qPCR,
861 using 18S as housekeeping gene and normalized to the NT average of each biological
862 experiment. Alternatively, at 48 hpt cells were infected with **D)** a 2022 IAV isolate of H1N1
863 (A/Burlington/UVM-0478/2022) or **E)** H3N2 (A/Burlington/UVM-1927/2022) subtype at an
864 MOI of 1. Viral supernatants were collected at 16 hpi and titered by plaque assay (PFU;
865 plaque forming unit). Mean +/- SEM of relative PFU (normalized to the NT average of each
866 biological experiment) is plotted. Statistical comparisons (D, E) were done using Welch's
867 one way ANOVA with Dunnett's multiple comparisons, [*($p<0.05$), **($p<0.01$), ***($p<0.001$),
868 ****($p<0.0001$)]. N=6 from three biological experiments (C), N=6 from three biological
869 experiments (D), and N=8 from four biological experiments (E) are shown.
870
871

Fig 2

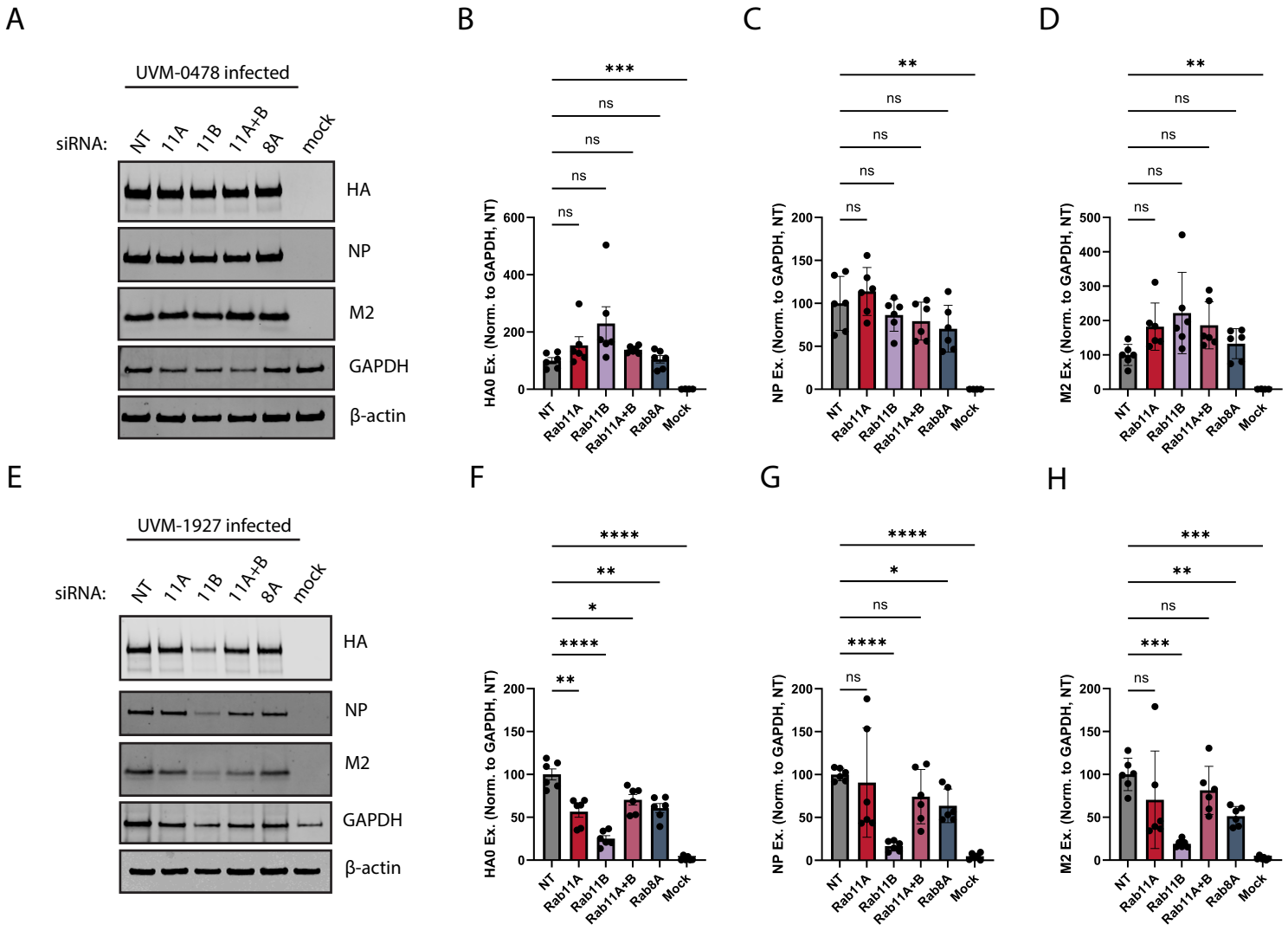
A
UVM-0478 infected
siRNA:
NT
11A
11B
11A+B
8A
mock
HA
NP
M2
GAPDH
β-actin
B
HA0 Ex. (Norm. to GAPDH, NT)
C
NP Ex. (Norm. to GAPDH, NT)
D
M2 Ex. (Norm. to GAPDH, NT)
E
UVM-1927 infected
F
G
H
Rab11A
Rab11B
Rab11A+B
Rab8A
Mock
ns

872 **Figure 2. Rab11B is required early in the life cycle of a recent H3N2 IAV isolate.**

873 A549 cells were treated with siRNAs targeting Rab11A, Rab11B (singly and in combination),
874 Rab8A or a non-targeting control, 48 hpt cells were infected with **A)** 2022 IAV isolate of
875 H1N1 (A/Burlington/UVM-0478/2022) at an MOI of 1, or mock infected. 16 hpi cell lysates
876 were collected and visualized by SDS-PAGE and western blot using rabbit anti-HA and anti-
877 GAPDH antibodies in addition to mouse anti-NP and anti-M2 antibodies. Expression of **B)**
878 HA, **C)** NP, and **D)** M2 was quantified and normalized to GAPDH levels and the NT control.
879 Alternatively, cells were infected with **E)** 2022 IAV isolate of H3N2 (A/Burlington/UVM-
880 1927/2022) at an MOI of 1, or mock infected. 16 hpi cell lysates were collected and
881 visualized by SDS-PAGE and western blot using rabbit anti-HA and anti-GAPDH antibodies
882 in addition to mouse anti-NP and anti-M2 antibodies. Expression of **F)** HA, **G)** NP, and **H)** M2
883 was quantified and normalized to GAPDH levels and the average NT control for each
884 biological replicate, quantification from six technical replicates (three biological
885 experiments) is shown. Mean +/- SEM is plotted. Statistical comparisons (B, C, D, F, G, H)
886 were done using the Welch's one way ANOVA with Dunnett's multiple comparisons
887 [*($p<0.05$), **($p<0.01$), ***($p<0.001$), ****($p<0.0001$)].
888
889
890

Fig 3

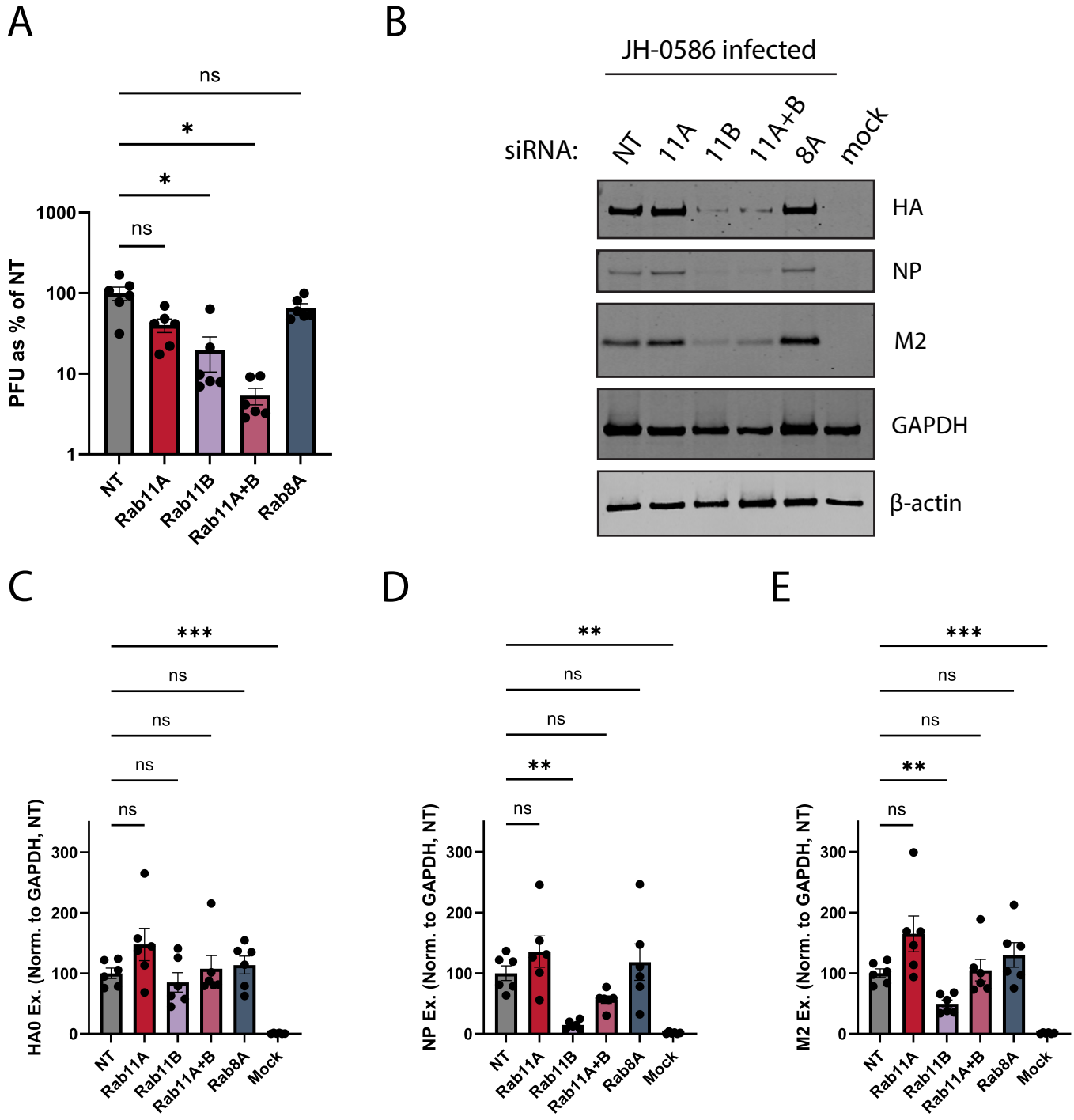
A
ns
*
*
ns
1000
100
10
1
PFU as % of NT
NT
Rab11A
Rab11B
Rab11A+B
Rab8A
B
JH-0586 infected
siRNA:
NT
11A
11B
11A+B
8A
mock
HA
NP
M2
GAPDH
β-actin
C
***
ns
ns
ns
ns
300
200
100
0
HA0 Ex. (Norm. to GAPDH, NT)
NT
Rab11A
Rab11B
Rab11A+B
Rab8A
Mock
D
**
ns
ns
**
ns
300
200
100
0
NP Ex. (Norm. to GAPDH, NT)
NT
Rab11A
Rab11B
Rab11A+B
Rab8A
Mock
E
***
ns
ns
**
ns
300
200
100
0
M2 Ex. (Norm. to GAPDH, NT)
NT
Rab11A
Rab11B
Rab11A+B
Rab8A
Mock

891 **Figure 3. Multiple H3N2 isolates depend on Rab11B early in IAV infection.**

892 A549 cells were treated with siRNAs targeting Rab11A, Rab11B (singly and in combination),
893 Rab8A or a non-targeting control, 48 hpt cells were infected with 2022 IAV isolate of H3N2
894 (A/Baltimore/JH-0586/2022) at an MOI of 1, or mock infected. **A)** 16 hpi viral supernatants
895 were collected and titered by plaque assay (PFU; plaque forming unit). **B)** Simultaneously,
896 cell lysates were collected and visualized by SDS-PAGE and western blot using rabbit anti-
897 HA and anti-GAPDH antibodies in addition to mouse anti-NP and anti-M2 antibodies.
898 Expression of viral proteins was quantified and normalized to GAPDH levels and the
899 average of the NT controls for each biological replicate and is shown for **C)** HA0, **D)** NP and
900 **E)** M2. Mean +/- SEM is plotted, normalized to the average of the NT control in each
901 biological experiment N=6 from three biological experiments. Statistical comparisons (A,
902 C, D, E) were done using Welch's one way ANOVA with Dunnett's multiple comparisons
903 [*($p<0.05$), **($p<0.01$), ***($p<0.001$)].
904
905

Fig 4

A

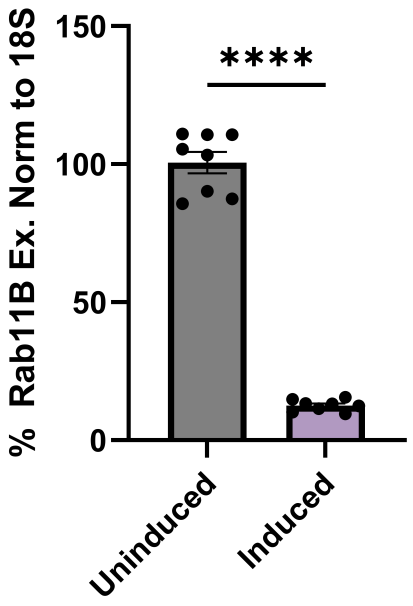
% Rab11B Ex. Norm to 18S
150
100
50
0
****
Uninduced
Induced

B

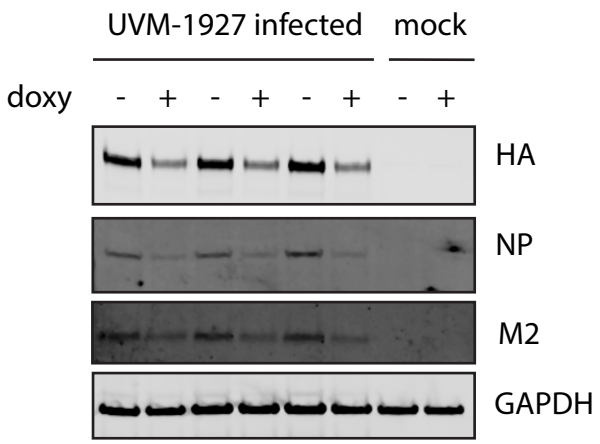
UVM-1927 infected
mock
doxy
- + - + - + - +
HA
NP
M2
GAPDH

C

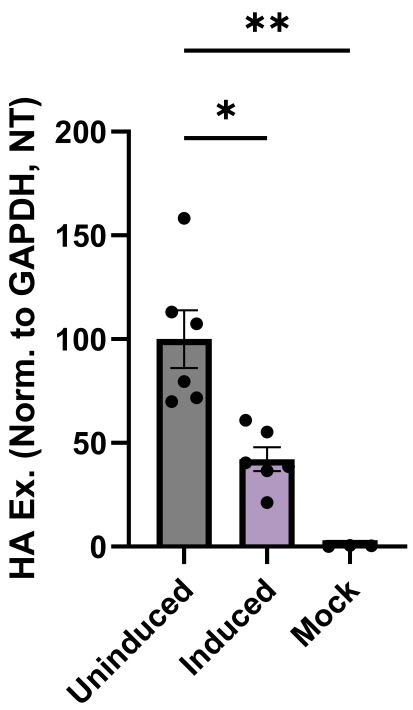
HA Ex. (Norm. to GAPDH, NT)
200
150
100
50
0
**
*
Uninduced
Induced
Mock

D

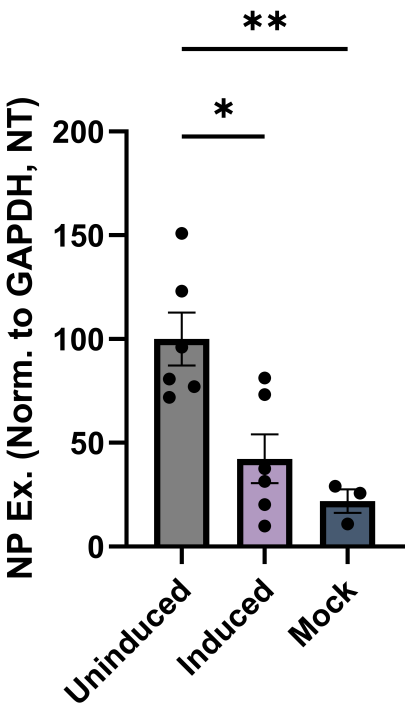
NP Ex. (Norm. to GAPDH, NT)
200
150
100
50
0
**
*
Uninduced
Induced
Mock

E

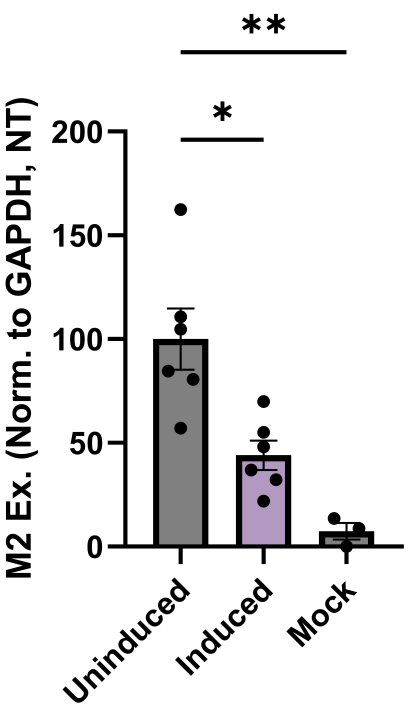
M2 Ex. (Norm. to GAPDH, NT)
200
150
100
50
0
**
*
Uninduced
Induced
Mock

906 **Figure 4. Rab11B is required early in the H3N2 life cycle in club (H441) cells**
907 **A)** H441 cells were transduced with a lentivirus to stably express an inducible shRNA
908 targeting Rab11B. Cells were treated (induced) or not (uninduced) with doxycycline to
909 induce shRNA expression, and 72 hours later RNA was harvested. Rab11B gene expression
910 was determined by RT-qPCR, using 18S as housekeeping gene and normalized to the
911 uninduced average of each biological experiment. **B)** Alternatively, cells were infected with
912 A/Burlington/UVM-1927/2022 or mock infected. 16 hpi cell lysates were collected and
913 visualized by SDS-PAGE and western blot using rabbit anti-HA and anti-GAPDH antibodies
914 in addition to mouse anti-NP and anti-M2 antibodies. Expression of **C)** HA, **D)** NP, and **E)** M2
915 was quantified and normalized to GAPDH levels and the average of the uninduced controls.
916 Quantification from six technical replicates (three biological experiments) is shown. Mean
917 +/- SEM is plotted. Statistical comparisons done using Welch's T-test (A) and Welch's one
918 way ANOVA with Dunnett's multiple comparisons (C, D, E) [*($p<0.05$), **($p<0.01$),
919 ****($p<0.0001$)].
920
921
922
923
924
925
926
927
928
929
930
931
932
933
934

Fig 5

A

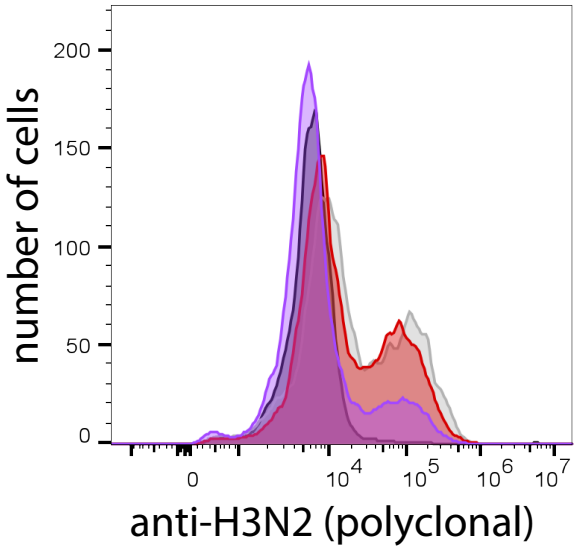

Color	Sample Name	Count
	Uninfected	5907
	NT control	6129
	Rab11A KD	6391
	Rab11B KD	4202

B

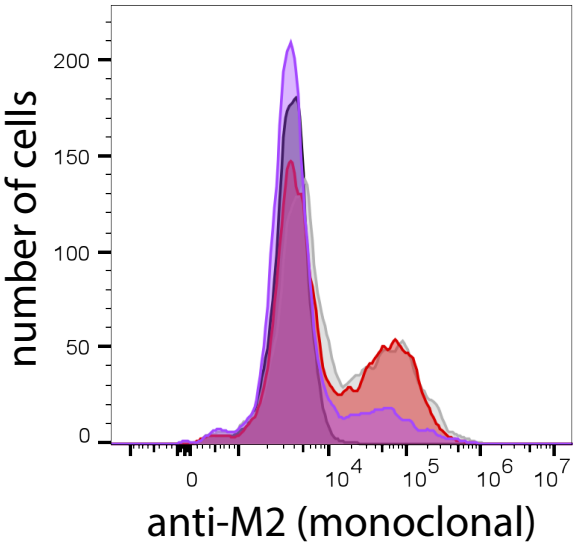

Color	Sample Name	Count
	Uninfected	5907
	NT control	6129
	Rab11A KD	6391
	Rab11B KD	4202

C

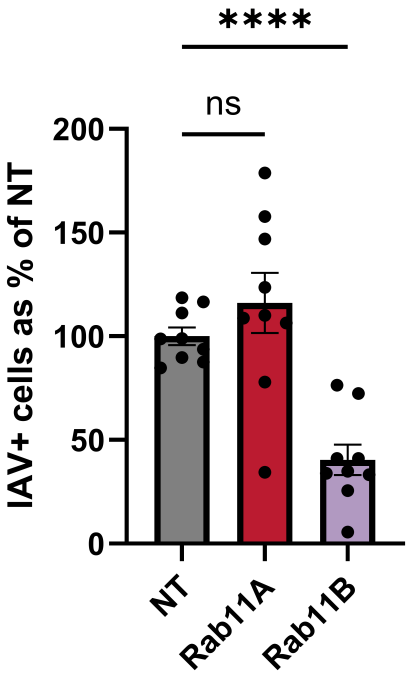

D

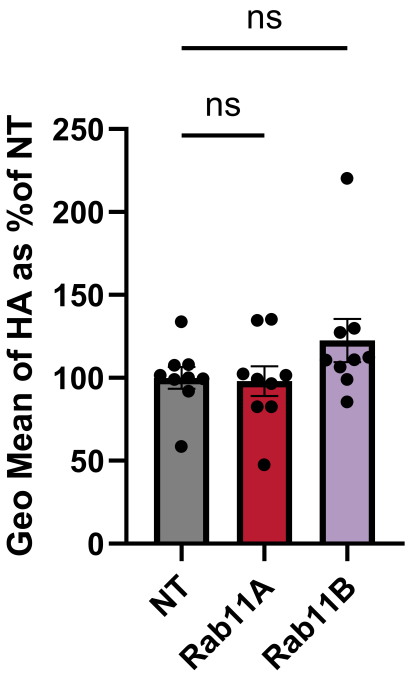

E

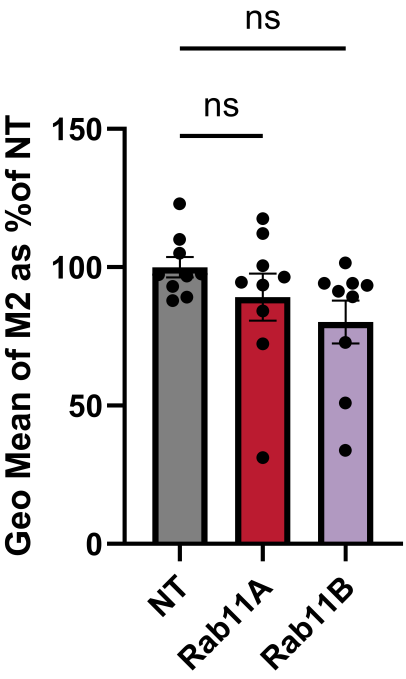

935 **Figure 5. Loss of Rab11B decreases the number of H3N2 IAV infected cells rather than**
936 **their protein expression.**
937 A549 cells were treated with siRNAs targeting Rab11A, Rab11B or a non-targeting control,
938 48 hpt cells were infected with 2022 IAV isolate of H3N2 (A/Burlington/UVM-1927/2022) at
939 an MOI of 1, or mock infected. 16 hours post infection cells were washed with PBS,
940 trypsinized, fixed and stained for flow cytometry analysis to determine total
941 (intracellular/extracellular) staining using **A)** anti-H3N2 or **B)** anti-M2 antibodies. **C)** The
942 percent of double $HA^+/M2^+$ cells in each experiment was determined using the mock
943 control to determine background staining levels. The geographic mean of **D)** HA or **E)** M2
944 expression in the infected ($HA^+/M2^+$) cell population, normalized to that of the NT infected
945 population is shown. Mean +/- SEM is plotted, normalized to the average of the NT control
946 in each biological experiment, N=9 from three biological experiments. Statistical
947 comparisons (C, D, E) done using Welch's one way ANOVA with Dunnett's multiple
948 comparisons [****($p<0.0001$)].
949
950

Fig 6

A

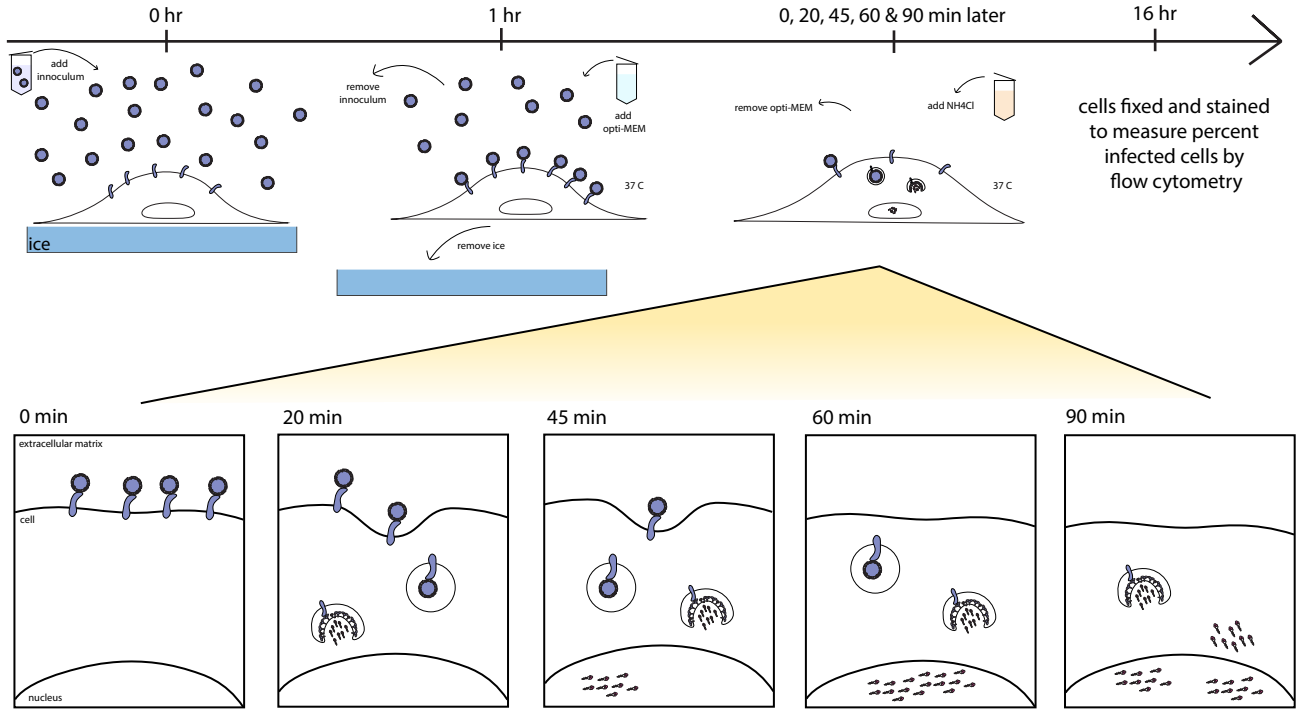

B

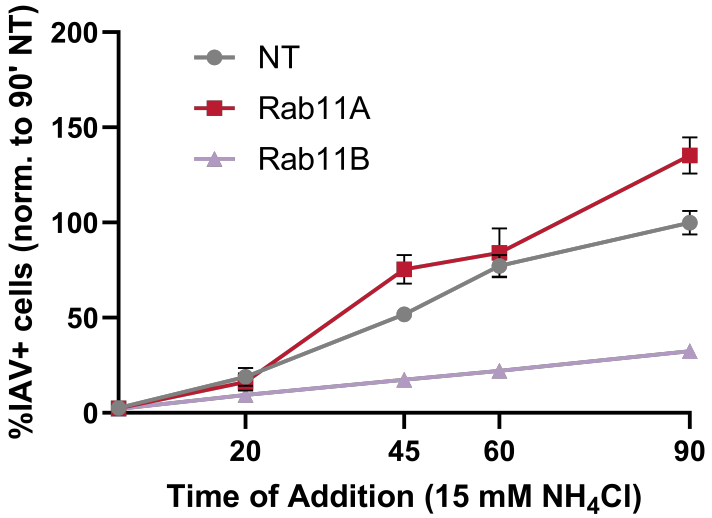

C

Timepoint	Rab KD	Summary	Adjusted P value
0	NT vs 11A	ns	0.9919
	NT vs 11B	ns	0.908
20	NT vs 11A	ns	0.8842
	NT vs 11B	ns	0.1759
45	NT vs 11A	*	0.0426
	NT vs 11B	****	<0.0001
60	NT vs 11A	ns	0.8442
	NT vs 11B	***	0.0002
90	NT vs 11A	*	0.026
	NT vs 11B	****	<0.0001

D

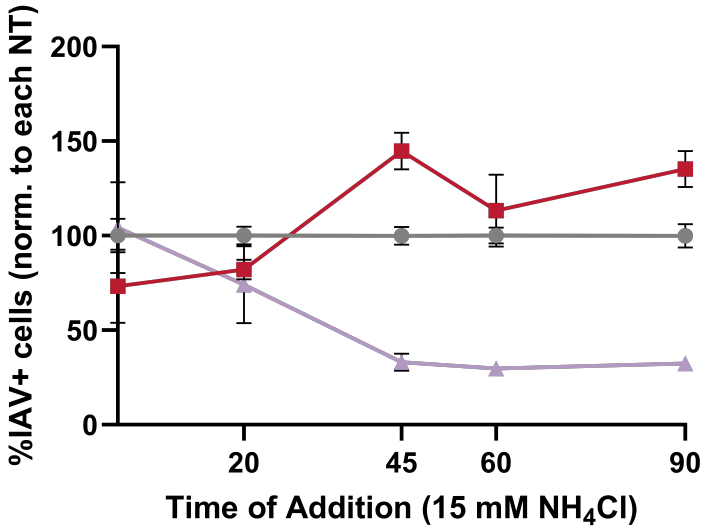

E

Timepoint	Rab KD	Summary	Adjusted P value
45 vs 60	Rab11B	ns	0.6376
45 vs 90	Rab11B	ns	0.9996
60 vs 90	Rab11B	ns	0.8476

951 **Figure 6. Loss of Rab11B delays the entry kinetics of the H3N2 IAV subtype**
952 **A)** A549 cells were treated with siRNAs targeting Rab11A, Rab11B or a non-targeting
953 control, 48 hpt cells were infected with 2022 IAV isolate of H3N2 (A/Burlington/UVM-
954 1927/2022) at an MOI of 1, or mock infected. At the indicated times (0, 20, 45, 60 or 90
955 minutes) post infection, viral overlay was removed and replaced with 15 mM NH_4Cl (to
956 prevent endosomal acidification and thus fusion of internalized virions) for the remainder
957 of the infection. 16 hours post inoculation cells were washed with PBS, trypsinized, fixed
958 and stained for flow cytometry analysis to determine total (intracellular as well as
959 extracellular) staining using anti-HA or anti-M2 antibodies. The percent of $HA^+/M2^+$ cells in
960 each experiment was determined using the mock control to determine background
961 staining levels. Mean +/- SEM is plotted, normalized to the average of the NT control for
962 each biological experiment **B)** at 90 minutes or **D)** at each timepoint. **C)** Statistical
963 comparisons of Rab11A or Rab11B depleted conditions vs the NT control were conducted
964 using a two-way ANOVA with Dunnett's multiple comparisons test and p values are
965 reported. **E)** Statistical comparisons of the Rab11B depleted condition over time were
966 conducted using a two-way ANOVA with Tukey's multiple comparisons test and p values
967 are reported. N=6 replicates from three biological experiments, [*($p<0.05$), ***($p<0.001$),
968 ****($p<0.0001$)].
969
970

Fig 7

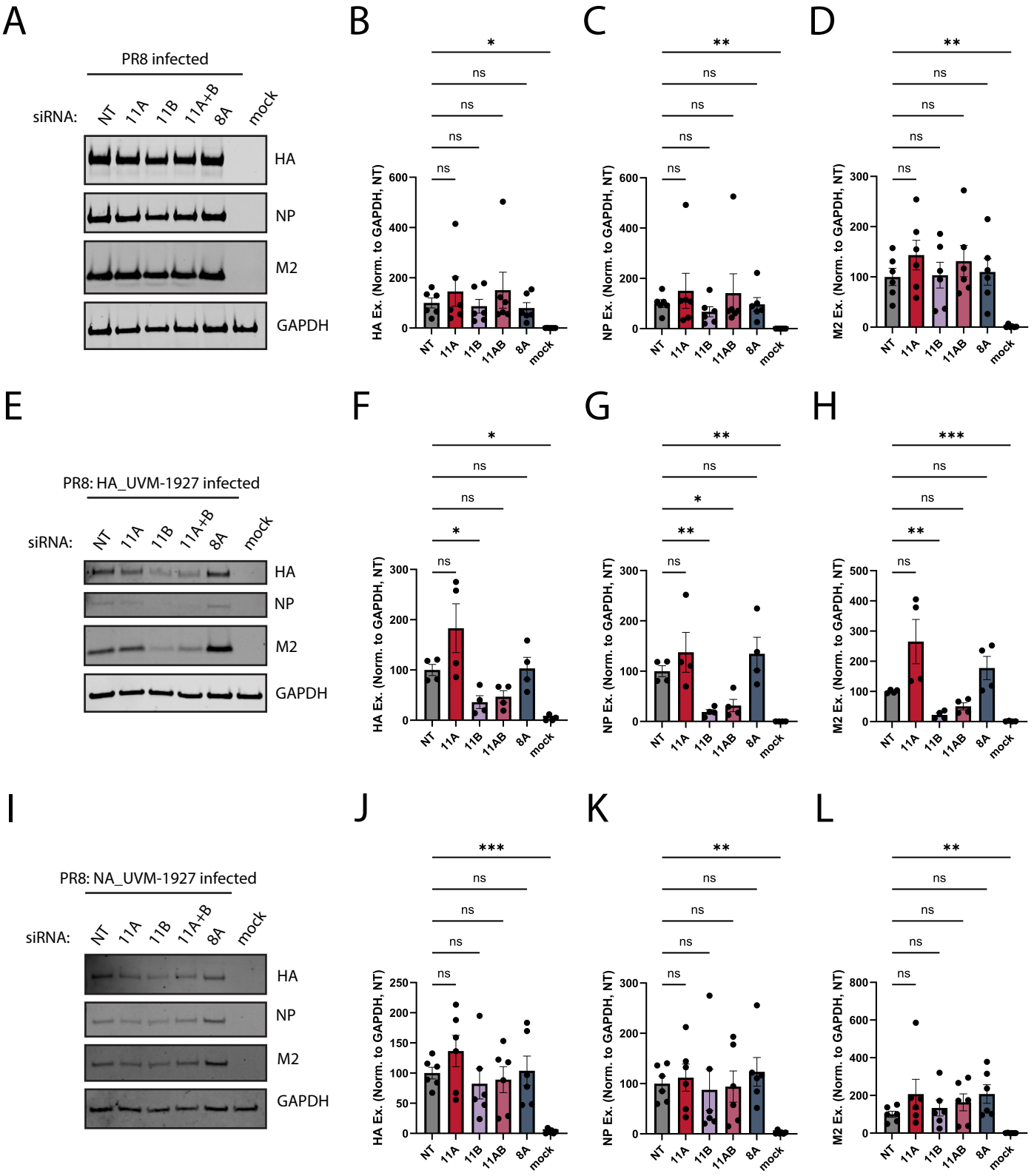
A
PR8 infected
siRNA: NT 11A 11B 11A+B 8A mock
HA
NP
M2
GAPDH
B
HA Ex. (Norm. to GAPDH, NT)
C
NP Ex. (Norm. to GAPDH, NT)
D
M2 Ex. (Norm. to GAPDH, NT)
E
PR8: HA_UVM-1927 infected
F
G
H
I
PR8: NA_UVM-1927 infected
J
K
L
NT 11A 11B 11AB 8A mock
ns
*
**
***

971 **Figure 7. H3N2 dependence on Rab11B early in infection can be mapped to the HA**
972 **gene.**
973 A549 cells were treated with siRNAs targeting Rab11A, Rab11B (singly and in combination),
974 Rab8A or a non-targeting control, 48 hpt cells were infected with **A)** A/Puerto Rico/8/1934
975 (PR8), **E)** a reverse genetics derived 7+1 reassortment containing the HA gene of UVM-1927
976 (PR8:HA UVM-1927) or **I)** a reverse genetics derived 7+1 reassortment containing the NA
977 gene of UVM-1927 (PR8:NA UVM-1927) at an MOI of 1, or mock infected. 16 hpi, cell lysates
978 were collected and visualized by SDS-PAGE and western blot using rabbit anti-HA and anti-
979 GAPDH antibodies in addition to mouse anti-NP and anti-M2 antibodies. Expression of viral
980 proteins was quantified and normalized to GAPDH levels and the average of the NT
981 controls for each biological replicate is shown for PR8 (**B, C, D**), PR8:HA UVM-1927 (**F, G, H**)
982 and PR8:NA UVM-1927 (**J, K, L**). (HA0, **D)** NP and **E)** M2. Mean +/- SEM is plotted, [*($p<0.05$),
983 **($p<0.01$), ***($p<0.001$), ****($p<0.0001$)], N=6 from three biological experiments (B, C, D,
984 J, K, L) or 4 from two biological experiments (F, G, H). Statistical comparisons done using
985 Welch's one way ANOVA with Dunnett's multiple comparisons.
986
987
988
989
990
991
992
993
994
995
996
997
998

Fig 8

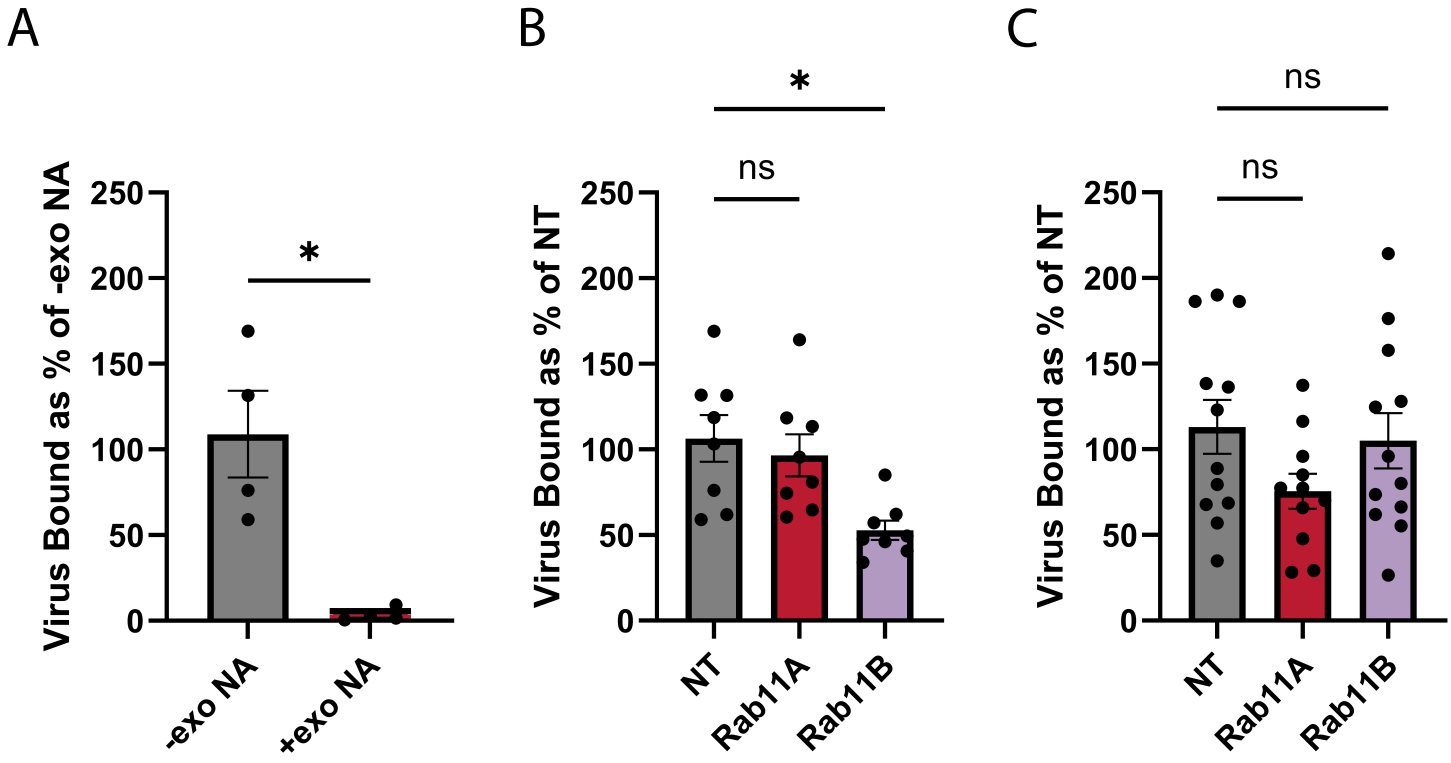
A
B
C
Virus Bound as % of -exo NA
Virus Bound as % of NT
Virus Bound as % of NT
250
200
150
100
50
0
*
ns
*
ns
ns
-exo NA
+exo NA
NT
Rab11A
Rab11B
NT
Rab11A
Rab11B

999 **Figure 8. Rab11B is required for efficient binding of H3N2 but not H1N1 virions to the**
1000 **cell surface.**
1001 A549 cells were prechilled on ice after which cold virus (A/Burlington/UVM-1927/2022
1002 [H3N2] at an MOI of 1) was bound to cells for one hour to synchronize binding. Cells were
1003 washed three times with ice cold PBS to remove unbound virus, and total virion binding
1004 was determined by extracting RNA from each well and using RT-qPCR to determine relative
1005 levels of IAV RNA vs a housekeeping control (18S). **A)** Bound virions were stripped by
1006 treating cells with exogenous neuraminidase. Alternatively, cells were treated with siRNAs
1007 targeting Rab11A, Rab11B or a non-targeting control for 48 h before binding **B)** a H3N2
1008 (A/Burlington/UVM-1927/2022) or a **C)** A/Burlington/UVM-0478/2022 as above. Mean +/-
1009 SEM is plotted, normalized to the average of the NT control in each biological experiment
1010 [*($p<0.05$)], N=4 from two biological experiments **(A)**, N=8 from three biological
1011 experiments **(B),** N=11-12 from two biological experiments **(C).** Statistical comparisons
1012 done using the Welch's t Test (A) and the Brown-Forsythe and Welch ANOVA tests.
1013
1014

Fig 9

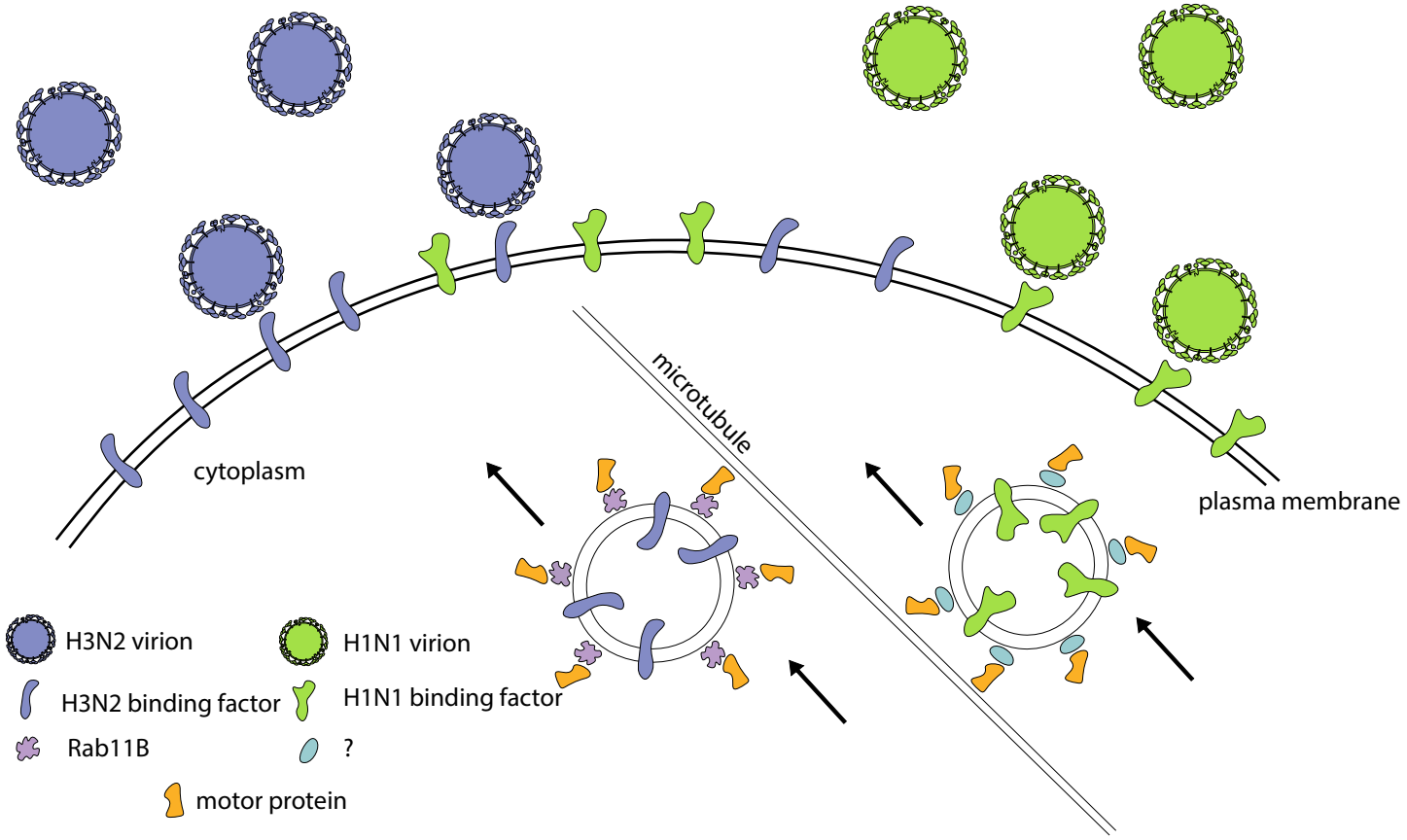
microtubule
cytoplasm
plasma membrane
H3N2 virion
H1N1 virion
H3N2 binding factor
H1N1 binding factor
Rab11B
?
motor protein

1015 **Figure 9. Rab11B may transport a H3N2 specific IAV binding receptor**

1016 We propose a model in which H3N2 virions (blue) bind to different cell surface proteins
1017 than H1N1 virions (green), and these cell surface proteins (putative binding 'receptors') are
1018 differentially transported by the Rab11B recycling pathway. In this framework, protein(s)
1019 required for H3N2 virions to bind are transported on Rab11B-positive vesicles, while the
1020 molecule(s) required for H1N1 binding are transported by a different (as of yet unidentified)
1021 cellular pathway that is independent of Rab11B.

1022

1023

1024

Fig. S1

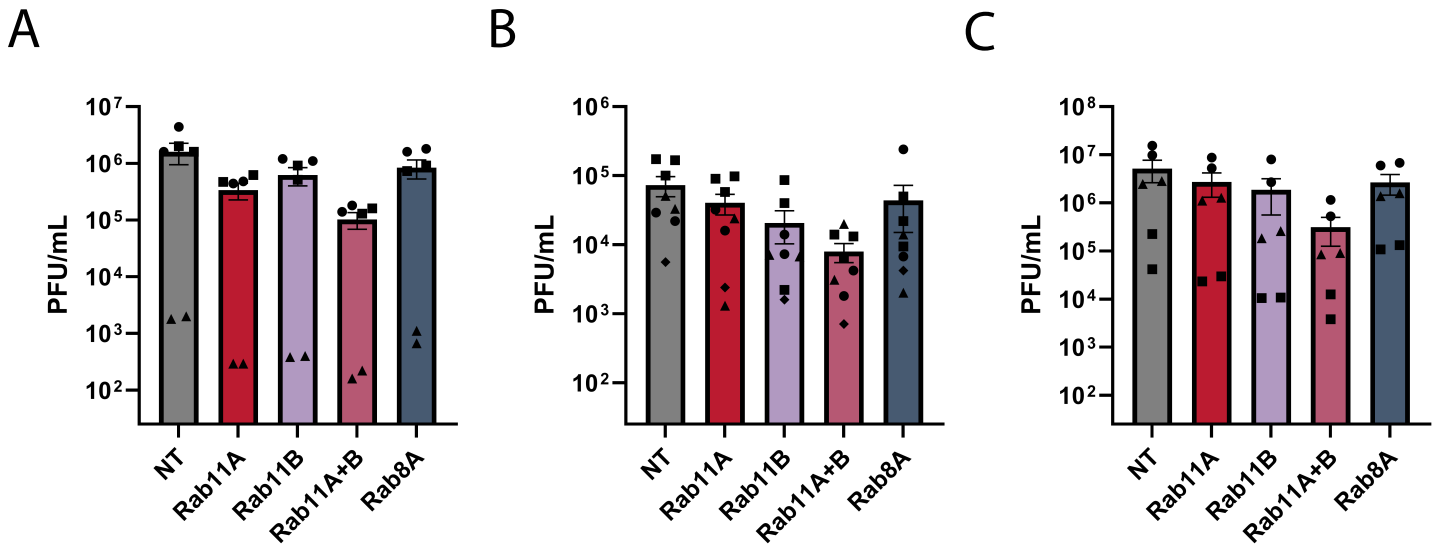
A
B
C
PFU/mL
10^7
10^6
10^5
10^4
10^3
10^2
10^8
NT
Rab11A
Rab11B
Rab11A+B
Rab8A

1025 **Figure S1. Raw titers of viral production in cells infected with recent H1N1 and H3N2**
1026 **influenza A isolates show Rab11A and Rab11B are consistently required for infectious**
1027 **virus production in both subtypes.**
1028 Raw titer data from cells infected with **A)** UVM-0478 (H1N1) [Figure 1B), **B)** UVM-1927
1029 (H3N2) [Figure 1C], or **C)** JH-0586 (H3N2) [Figure 2A] is presented here as PFU/mL.
1030 Biological replicates are distinguished by shape (■,◆,▲, or ●) with N=6 from three
1031 biological experiments (A, C) and N=8 from four biological experiments (B).
1032
1033

Fig. S2

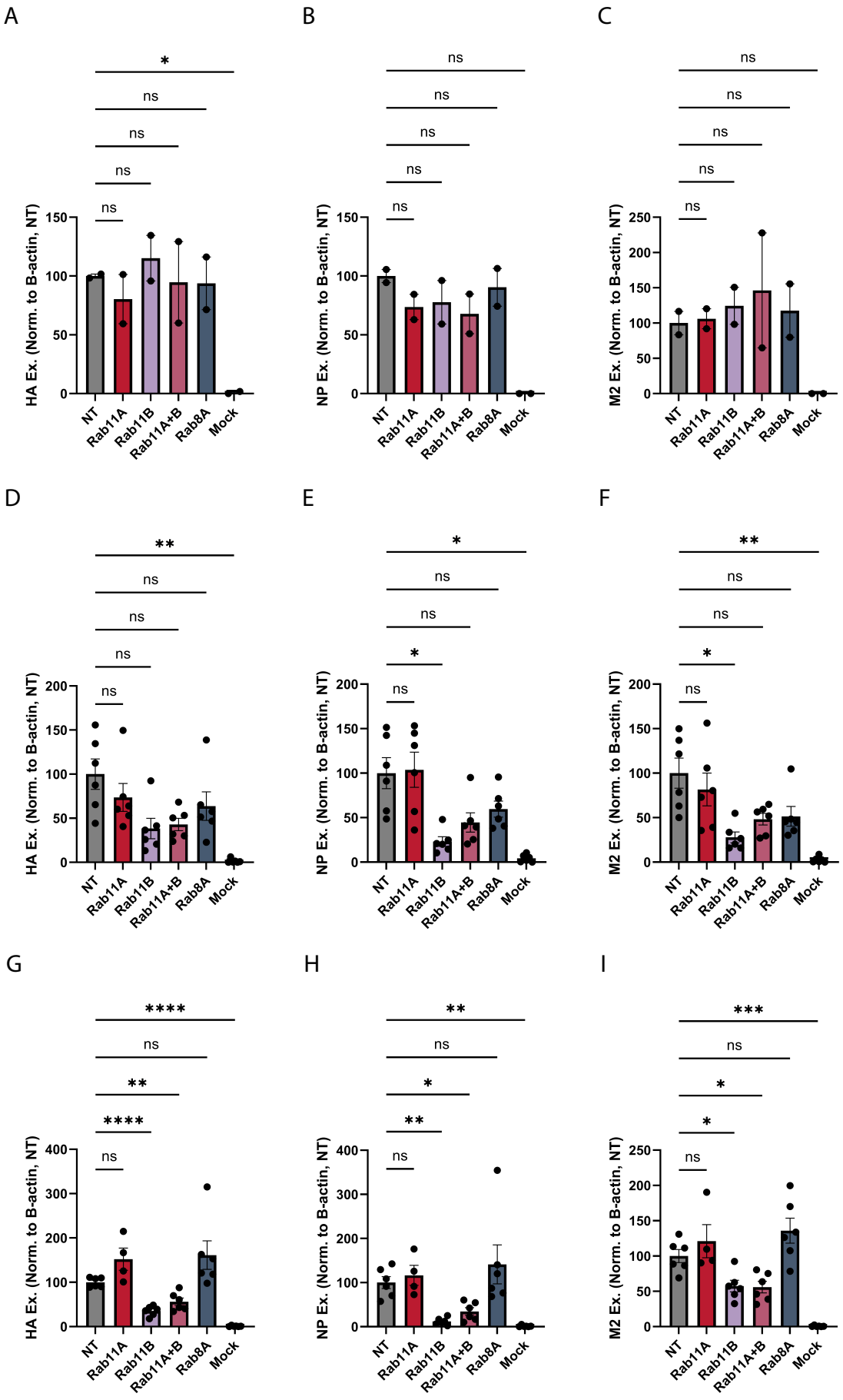
A
B
C
D
E
F
G
H
I
HA Ex. (Norm. to B-actin, NT)
NP Ex. (Norm. to B-actin, NT)
M2 Ex. (Norm. to B-actin, NT)
NT
Rab11A
Rab11B
Rab11A+B
Rab8A
Mock
ns
*
**
***
****

1034 **Figure S2. The dependence of H3N2 viral protein production in cells lacking Rab11B is**
1035 **seen with normalization to multiple cellular housekeeping genes.**
1036 Data presented in Figure 2 and Figure 3 was alternatively quantified here by normalizing to
1037 β-actin and the average of NT control for each biological replicate; **(A)** Figure 2B, **(B)** Figure
1038 2C, **(C)** Figure 2D, **(D)** Figure 2F, **(E)** Figure 2G, **(F)** Figure 2H, **(G)** Figure 3C, **(H)** Figure 3D, and
1039 **(I)** Figure 3E is shown for HA0 **(A, D, G)**, NP **(B, E, H)** and M2 **(C, F, I)**. Mean +/- SEM is
1040 plotted, N=2 from one biological experiment **(A-C)** and N=6 from three biological
1041 experiments **(D-I).** Statistical comparisons done using Welch's one way ANOVA with
1042 Dunnett's multiple comparisons [*($p<0.05$), **($p<0.01$), ***($p<0.001$), ****($p<0.0001$)].
1043
1044

Fig. S3

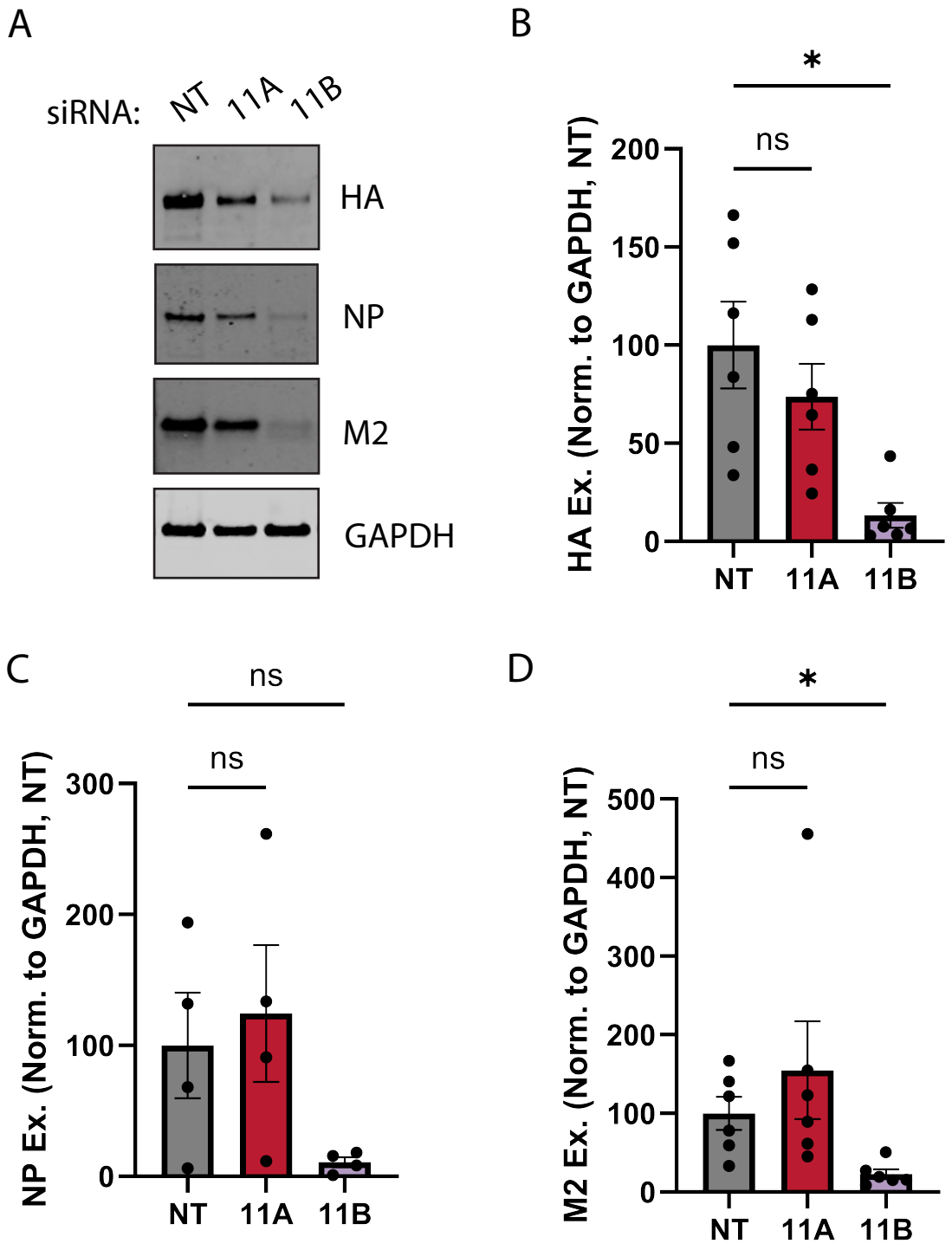
A
siRNA:
NT
11A
11B
HA
NP
M2
GAPDH
B
*
ns
HA Ex. (Norm. to GAPDH, NT)
200
150
100
50
0
NT
11A
11B
C
ns
ns
NP Ex. (Norm. to GAPDH, NT)
300
200
100
0
NT
11A
11B
D
*
ns
M2 Ex. (Norm. to GAPDH, NT)
500
400
300
200
100
0
NT
11A
11B

1045 **Figure S3. Rescue of Rab11B-dependent defect in H3N2 viral protein production in**
1046 **cells simultaneously depleted of Rab11A and Rab11B is not an artifact of knockdown**
1047 **efficiency.**
1048 A549 cells were treated with siRNAs targeting Rab11A, Rab11B or a non-targeting control at
1049 half the amount typically used (5nm instead of the standard 10 nm). 48 hpt cells were
1050 infected with UVM-1927 at an MOI of 1, or mock infected. **A)** 16 hpi cell lysates were
1051 collected and proteins visualized by SDS-PAGE and western blot using rabbit anti-HA and
1052 anti-GAPDH antibodies in addition to mouse anti-NP and anti-M2 antibodies. Expression of
1053 viral proteins was quantified and normalized to GAPDH levels and the average of the NT
1054 control for each biological replicate is shown for HA0 **(B)**, NP **(C)** and M2 **(D)**. Mean +/- SEM
1055 is plotted, N=6 from three biological experiments. Statistical comparisons done using
1056 Welch's one way ANOVA with Dunnett's multiple comparisons (*=$p<0.05$).
1057
1058
1059
1060
1061